Safeguarding genome integrity with small ubiquitin-like modifiers

Claessens, L.A.

Citation

Claessens, L. A. (2024, June 27). *Safeguarding genome integrity with small ubiquitin-like modifiers*. Retrieved from https://hdl.handle.net/1887/3765377

Chapter 4

Global non-covalent SUMO interaction networks reveal SUMO-dependent stabilization of the non-homologous end joining complex

Román González-Prieto[1], Karolin Eifler-Olivi [2], Laura A Claessens[1], Edwin Willemstein[1], Zhenyu Xiao[1], Cami M P Talavera Ormeno[3], Huib Ovaa[3], Helle D Ulrich[4], Alfred C O Vertegaal[1]

[1] Department of Cell and Chemical Biology, Leiden University Medical Center, Leiden, the Netherlands
[2] Department of Cell and Chemical Biology, Leiden University Medical Center, Leiden, the Netherlands; Institute of Molecular Biology, Mainz, Germany
[3] Department of Cell and Chemical Biology, Leiden University Medical Center, Leiden, the Netherlands; Oncode Institute, Leiden, the Netherlands
[4] Institute of Molecular Biology, Mainz, Germany

ABSTRACT

In contrast to our extensive knowledge on covalent small ubiquitin-like modifier (SUMO) target proteins, we are limited in our understanding of non-covalent SUMO-binding proteins. We identify interactors of different SUMO isoforms—monomeric SUMO1, monomeric SUMO2, or linear trimeric SUMO2 chains—using a mass spectrometry-based proteomics approach. We identify 379 proteins that bind to different SUMO isoforms, mainly in a preferential manner. Interestingly, XRCC4 is the only DNA repair protein in our screen with a preference for SUMO2 trimers over mono-SUMO2, as well as the only protein in our screen that belongs to the non-homologous end joining (NHEJ) DNA double-strand break repair pathway. A SUMO interaction motif (SIM) in XRCC4 regulates its recruitment to sites of DNA damage and phosphorylation of S320 by DNA-PKcs. Our data highlight the importance of non-covalent and covalent sumoylation for DNA double-strand break repair via the NHEJ pathway and provide a resource of SUMO isoform interactors.

Highlights

- Identification of 379 non-covalent interactors of SUMO1, SUMO2, or SUMO2 trimers
- Definition of an optimal high-affinity SUMO interaction motif (SIM)
- A functional SIM in XRCC4 regulates its recruitment to local sites of DNA damage
- A functional SIM in XRCC4 regulates phosphorylation of S320 by DNA-PKcs

INTRODUCTION

Post-translational modification of proteins regulates virtually all biological processes in a dynamic manner. These post-translational modifications include modification by small chemical groups, including phosphorylation, methylation, and acetylation, and modification by small proteins belonging to the ubiquitin family (Deribe et al., 2010). Ubiquitin can modify targets in a monomeric form as well as in a large variety of polymeric forms (Swatek and Komander, 2016). Extensive sets of enzymes mediate the conjugation and deconjugation of target proteins with these modifying groups. Kinases and ubiquitin ligases are classical examples of these particularly large sets of enzymes (Zheng and Shabek, 2017). Equally important for the transduction of these signals are the non-covalent interactors that are equipped with specific domains to recognize and bind modified proteins. Examples include the SH2 domain that recognizes phosphorylated-tyrosine residues (Pawson, 2004) and ubiquitin-binding motifs, including the ubiquitin-interacting motif (UIM), the ubiquitin-binding zinc finger (UBZ), and the ubiquitin binding in ABIN and NEMO (UBAN) domain (Husnjak and Dikic, 2012). Tandem ubiquitin binding domains enable the specific recognition of differential types of ubiquitin polymers.

The ubiquitin family is composed of ~1 dozen ubiquitin-like proteins, including Nedd8, small ubiquitin-like modifiers (SUMO), Interferon stimulated gene 15 (ISG15), ubiquitin-fold modifier 1 (UFM1), and autophagy-related modifiers ATG8 and ATG12 (Cappadocia and Lima, 2018). Here, we focus on signal transduction by SUMOs (Flotho and Melchior, 2013). Compared to ubiquitin, the enzymatic machinery that mediates its conjugation and deconjugation is of low complexity and includes the dimeric E1 SUMO activating enzyme (SAE); a single E2 (UBC9/UBE2I) and E3 ligases, including protein inhibitor of activated STAT1-4 (PIAS), RanBP2, and ZNF451. SUMO proteases are SENP1–3, SENP5–7, DESI1 and -2, and USPL1 (Hickey et al., 2012).

Conjugated SUMOs are predominantly located in nuclei, regulating nuclear processes, including transcription, replication, maintaining genome integrity, transport, and pre-mRNA splicing. Mice deficient for SUMO signaling die at the early post-implantation stage,

4

displaying nuclear aberrations, including altered nuclear bodies, nucleoli, and nuclear architecture, and mitotic problems including anaphase bridges (Nacerddine et al., 2005).

In the last 6 years, our knowledge regarding covalent SUMO target proteins has increased considerably as a result of progress in the proteomics approaches to enrich and identify these targets, including the conjugated lysines in these targets. Several thousand SUMO target proteins have been identified so far in a site-specific manner (Hendriks et al., 2017, 2018; Hendriks and Vertegaal, 2016; Tammsalu et al., 2014). SUMOs are conjugated to lysines in target proteins that are frequently located in the sumoylation consensus motif ψKxE (ψ is a residue with a large hydrophobic side chain) or the inverted motif [ED]xKψ under regular cell culture conditions (Hendriks et al., 2018; Matic et al., 2010). Extended sumoylation consensus motifs include the phosphorylation-dependent sumoylation motif (PDSM) (Hietakangas et al., 2006) and the negatively charged amino acid-dependent sumoylation motif (NDSM) (Yang et al., 2006). The SUMO proteome is dynamic and alters under stress conditions, including heat stress and blocking of the proteasome (Golebiowski et al., 2009; Liebelt et al., 2019). The ability of SUMO to co-regulate functionally related proteins has attracted considerable attention in the field (Jentsch and Psakhye, 2013; Johnson and Blobel, 1999; Psakhye and Jentsch, 2012). Mutating SUMO acceptor lysines in one individual target protein does not notably alter its functionality as long as other proteins in the network remain SUMO modified. Only upon the loss of sumoylation of a considerable set of functionally related proteins is loss of their functionality noted.

In contrast to our vast knowledge on covalent SUMO signaling, we are limited in our understanding of non-covalent SUMO signaling. Initial studies have uncovered a non-covalent SUMO interaction motif (SIM) that contains three large hydrophobic residues flanked by one or more acidic residues (Aguilar-Martinez et al., 2015; Hecker et al., 2006). These hydrophobic residues in SIMs form a parallel β sheet pairing with the β sheet in SUMO to mediate their interaction (Sekiyama et al., 2008). Furthermore, a ZZ zinc finger in HERC2 was found to enable SUMO interaction (Danielsen et al., 2012).

Interestingly, these SIMs play important roles in the assembly of promyelocytic leukemia protein (PML) nuclear bodies. The PML protein contains a SIM that may be important for nuclear body assembly and for the accumulation of SUMO in these bodies (Shen et al., 2006). Furthermore, oxidation-mediated PML multimerization is important as nucleation event for nuclear body formation (Sahin et al., 2014). Interestingly, these bodies can be assembled *in vitro* via phase separation when PML and SUMO are present (Banani et al., 2016). Furthermore, SIMs have been found in SUMO-targeted ubiquitin ligases (STUbLs) (Lescasse et al., 2013; Prudden et al., 2007). Multiple SIMs in these STUbLs enable their

interaction with poly-sumoylated proteins, which are subsequently ubiquitinated and degraded by the proteasome (Lallemand-Breitenbach et al., 2008; Tatham et al., 2008). STUbLs are important for the maintenance of genome stability (Galanty et al., 2012; Vyas et al., 2013; Yin et al., 2012) and primarily target auto-sumoylated SAE, UBC9 and SUMO E3 ligases for degradation (Kumar et al., 2017, Salas-Lloret et al., 2019).

Given the limited set of non-covalent SUMO interactors that is currently known, we set out to enrich these proteins from lysates using recombinant non-conjugatable SUMO1, SUMO2, and a SUMO2 trimer. This enabled us to identify large sets of proteins that preferentially interact with SUMO1, SUMO2, or SUMO2 trimers.

RESULTS

A non-covalent SUMO isoform-specific binding screen

Aiming to identify both common and differential non-covalent binders to mono-SUMO1, mono-SUMO2, and SUMO2 polymers, 10xHIS-tagged versions of SUMO1, SUMO2, and a linear triple SUMO2 fusion were recombinantly produced in *Escherichia coli*. These constructs lacked the SUMO C-terminal di-Gly motif to prevent covalent binding to target proteins. Next, the HIS-tagged SUMO variants were bound to nickel-nitrilotriacetic acid (Ni-NTA) beads and incubated with whole-cell extracts from HeLa cells. Uncoated Ni-NTA beads were used as negative control. While the HIS-SUMO1- and HIS-SUMO2-coated beads enabled the identification of SUMO monomer and multimer interacting proteins, the HIS-SUMO2 linear trimer fusion-coated beads enabled the identification of proteins that interacted with SUMO polymers. Subsequently, proteins binding to the different SUMO isoforms were eluted and trypsin digested. The resulting peptides were identified by liquid chromatography-tandem mass spectrometry (LC-MS/MS) analysis (Figure 1A). Elution with 8 M urea buffer enabled us to release the SUMO binding proteins from the beads without releasing the high amounts of SUMOs used, facilitating the identification of the interacting proteins by MS. Adding imidazole to the 8 M urea buffer further increased the elution of binding proteins together with the SUMO isoforms. Four independent biological replicates were performed (Figure S1A). Detection of RNF4 as an expected SUMO interactor served as a positive control. Furthermore, heatmap analysis of the identified proteins indicated that biological replicates clustered together by condition, indicating high reproducibility (Figure S1B).

Proteins binding to each of the different SUMO isoforms were identified and quantified. After removing common contaminants and non-consistently identified proteins, qualitative

and quantitative analyses were performed for 1,520 identified protein groups. Compared to the control sample, 379 proteins were identified to bind to SUMO1, SUMO2, and/or polySUMO2. A total of 83 proteins bound significantly to SUMO1, 279 to SUMO2, and 247 to polySUMO2 in a preferential manner (Figure 1B; Data S1, Dataset 1). While 102 and 90 proteins were able to exclusively bind to either monomeric-SUMO2 or SUMO2 polymers, respectively, only 8 were exclusively bound to monomeric SUMO1; 51 of the 379 interacting proteins were able to bind SUMO irrespective of its isoform (Figure 1C; Data S1, Dataset 1).

Interacting proteins with a preference for SUMO1, SUMO2, or SUMO2 trimer

To study interactions between the 83 SUMO1-binding proteins in more detail (Figure 1B; Data S1, Dataset 1), we performed STRING analysis (Szklarczyk et al., 2015), followed by a search for highly interconnected clusters (Figure 2A). We identified clusters of proteins corresponding to the nuclear lamina, PML bodies, participating in sumoylation or mRNA splicing, and RNA metabolic processes. Furthermore, Gene Ontology analysis was performed for the 83 SUMO1-binding proteins (Figure 2B; Data S1, Dataset 2). Consistently, SUMO binding and SUMO transferase activities were the most highly enriched molecular functions and RNA processing was the most highly enriched biological process.

We then performed STRING analysis for the 279 SUMO2-binding proteins (Figure S2), and searched for highly interconnected clusters (Figure 2C). Similar to SUMO1-binding proteins, sumoylation and RNA metabolic processes-related clusters were identified. Moreover, a cluster of DNA damage response-related proteins was also identified, which was not present among the SUMO1-binding proteins. Furthermore, Gene Ontology analysis identified several different DNA repair pathways as biological processes and binding to different types of DNA lesions as molecular function (Figure 2D; Data S1, Dataset 3).

STRING analysis was also performed for the 247 proteins binding to SUMO2 trimers (Figure S3A) to search for highly interconnected clusters (Figure 3A). As previously identified for SUMO1 and SUMO2, protein sumoylation and RNA metabolic processes were identified, and, similarly to SUMO2, a DNA damage response protein cluster was also identified. Remarkably, other protein clusters were also identified compared to SUMO1 or SUMO2 monomers, including mRNA splicing, chromatin organization, and microtubule-based movement clusters. Gene Ontology analysis of the SUMO2 trimer binders revealed several DNA damage response pathways as significantly enriched biological processes and molecular functions related to sumoylation, DNA repair, and chromatin modification (Figure 3B; Data S1, Dataset 4). The affinity of some of the SUMO2 trimer binding proteins identified by MS was confirmed by immunoblotting (Figure S3B).
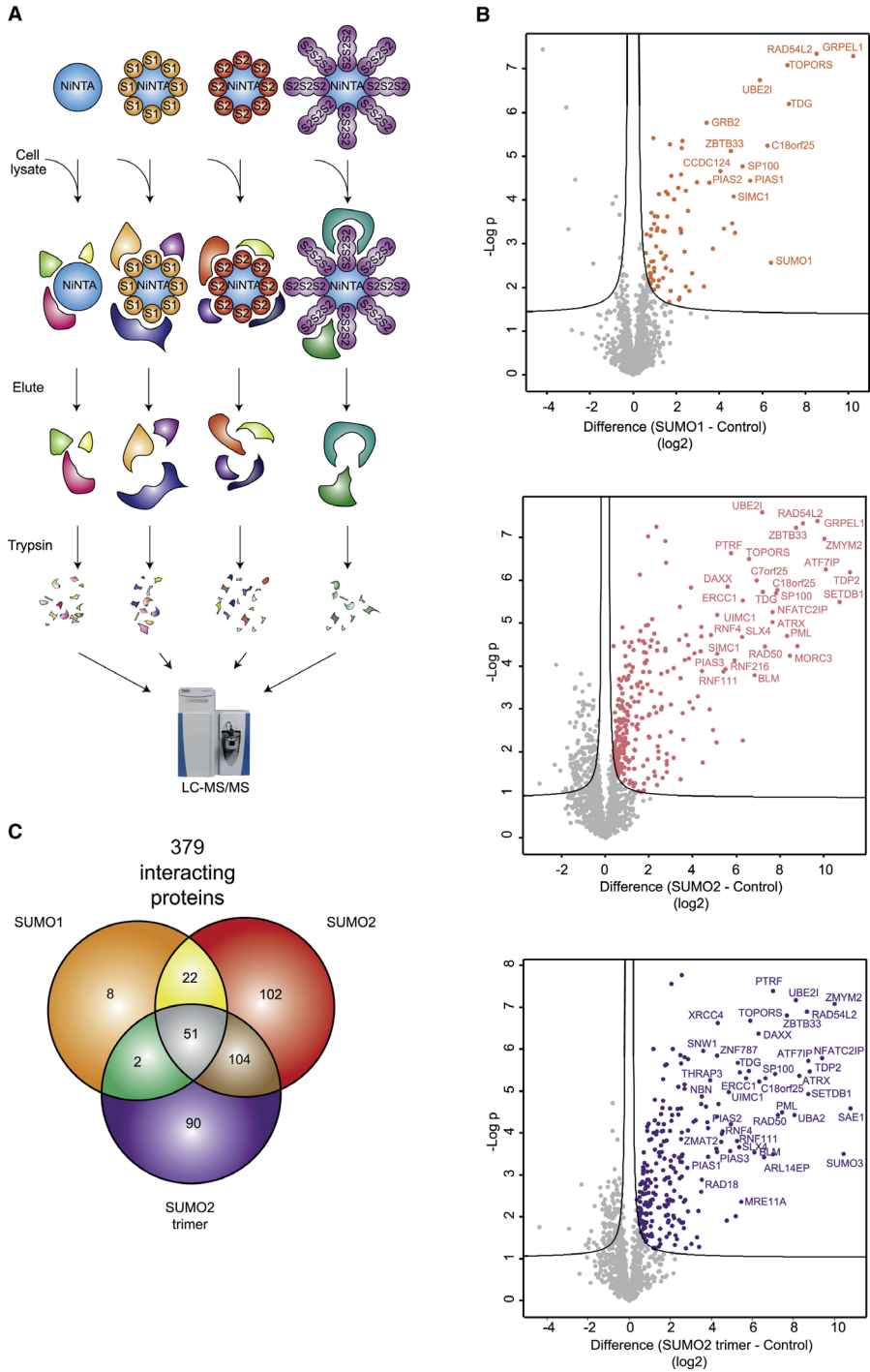
Figure 1. Purification and identification of SUMO isoform-specific binders.

Figure 1 (continued).
(A) Experimental setup. Ni-NTA beads as control or coated with either SUMO1, SUMO2, or SUMO2 trimer were incubated with a HeLa lysate under native conditions and SUMO interactors were purified. Subsequently, SUMO binders were eluted, trypsin digested, and identified by mass spectrometry. **(B)** Volcano plots depicting the identified interactors for SUMO1, SUMO2, or SUMO2 trimer. Each dot represents a protein; each colored dot in orange, red, or purple represents a significantly enriched protein compared to the control beads in SUMO1, SUMO2, or SUMO2 trimer-coated beads, respectively, from 4 independent experiments (Student's t test with a permutation-based false discovery rate [FDR] of 0.05 and S0 = 0.1). **(C)** Venn diagram representing the 379 identified interacting proteins with either SUMO1, SUMO2, or SUMO2 trimer.
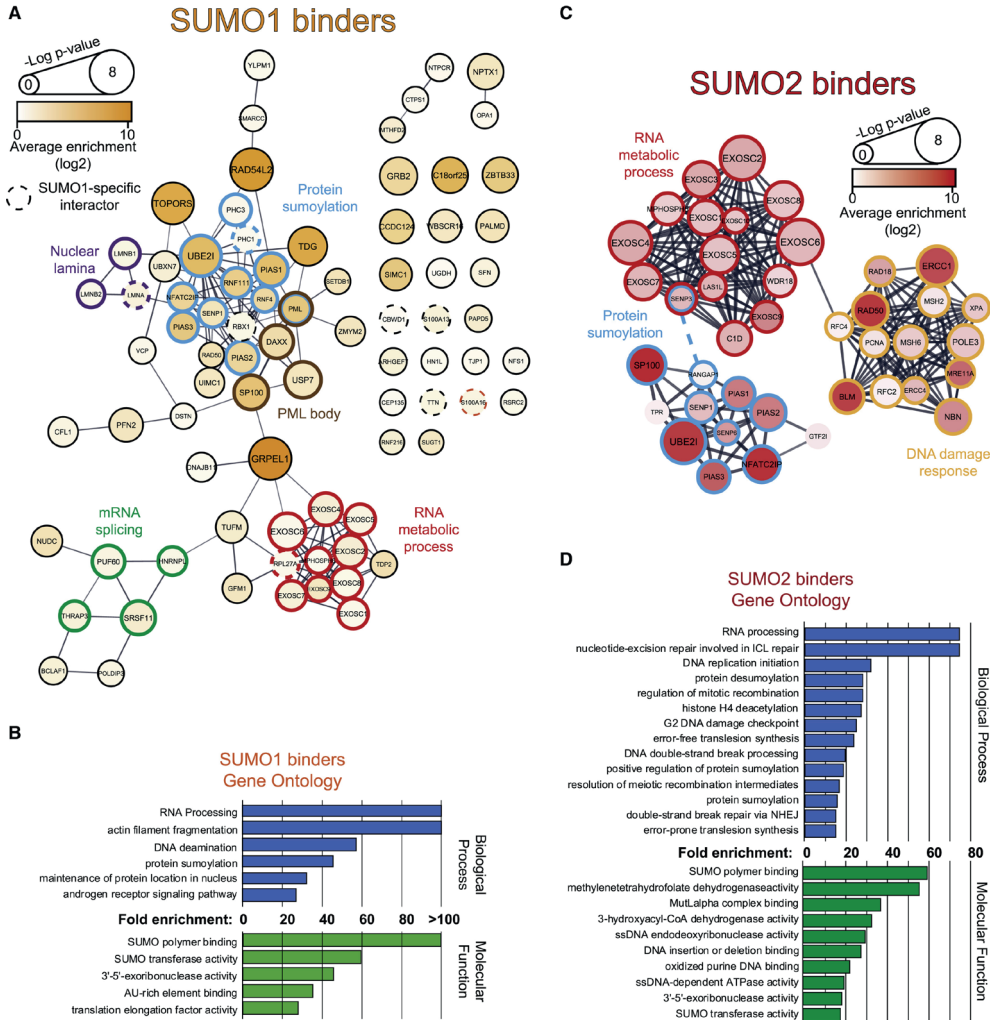

Figure 2. Analysis of SUMO1 and SUMO2 binders. **(A)** STRING network analysis of SUMO1 binders including connected and unconnected nodes. The size of the circle represents the –log p value of the identification as binder. Orange color intensity represents the average enrichment compared to control beads. Dotted lines indicate that the protein is a SUMO1-specific binder. Colored outlines of the circles represent a highly interconnected cluster for a specific Gene Ontology term.

Figure 2 *(continued).*
(B) Curated Gene Ontology analysis of SUMO1 binders regarding biological process and molecular function. **(C)** Highly interconnected clusters of SUMO2 binders extracted from STRING analysis. Red color intensity represents the average enrichment compared to control beads. Colored outlines of the circles represent a highly interconnected cluster for a specific Gene Ontology term. **(D)** Curated Gene Ontology analysis of SUMO2 binders regarding biological process and molecular function.

Overlap between SUMO binding proteins and SUMO substrates

The SUMO proteome has been intensively studied, achieving the identification of >40,000 SUMO acceptor lysines in >6,000 proteins so far (Hendriks et al., 2017). We investigated which fractions of the SUMO1, SUMO2, or SUMO2 trimer binding proteins were also identified as covalent SUMO substrates (Figure 4A). This percentage was close to 90% in all cases. However, when we looked at the average amount of sumoylation sites per protein comparing SUMO1, SUMO2, or SUMO2 trimer-binding proteins (Figure 4B; Data S1, Dataset 5), we observed that this number was significantly higher in SUMO2 trimer-binding proteins, indicating that proteins binding to SUMO2 chains are more extensively sumoylated.

We decided to investigate whether this was also true for SUMO1-conjugated proteins. However, the amount and size of available datasets for SUMO1 sites are scarce compared to SUMO2 sites. In a previous study, using a SUMO1-T95R mutant, Impens et al. (2014) identified 295 SUMO1 sites. We aimed to complement this study and increase the number of identified SUMO1 sites. Using a similar strategy to the one we previously used for SUMO2 sites (Hendriks et al., 2014), we used a 10xHIS-tagged lysine-deficient Q92R SUMO1 mutant. HIS-SUMO1-modified proteins were purified using Ni-NTA beads and subsequently digested with the protease LysC. After a second Ni-NTA-mediated HIS purification, SUMO1 conjugates attached to the LysC remnant containing the sumoylated lysines were treated with trypsin, resulting in peptides bearing the EQTGG remnant attached to the SUMO1-conjugated lysine, which were subsequently identified by MS (Figure 4C). Using this strategy, we identified 315 SUMO1 sites on 172 proteins, 55 of the identified sites of which were overlapping with the ones that had already been identified (Impens et al., 2014) (Figure 4D; Data S1, Datasets 6 and 7). Considering the identified SUMO1 sites from both Impens et al. (2014) and this study (Data S1, Dataset 7), the percentage of non-covalent SUMO1 binders that are also identified as covalent SUMO1 target proteins is high (Figure 4E; Data S1, Dataset 8).
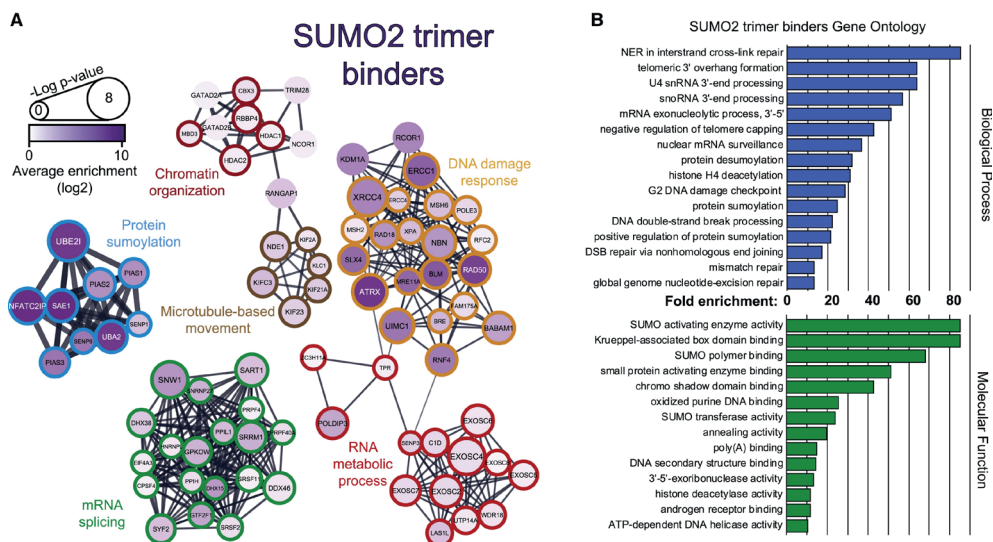
Figure 3. Analysis of SUMO2 trimer binders. (A) Highly interconnected clusters extracted from STRING analysis of SUMO2 trimer binders. Purple color intensity represents the average enrichment compared to control beads. Colored outlines of the circles represent a highly interconnected cluster for a specific Gene Ontology term. **(B)** Curated Gene Ontology analysis of SUMO2 trimer binders regarding biological process and molecular function.

Toward high-affinity SIMs

We evaluated whether SUMO binding proteins have preferential affinity for SUMO1 or SUMO2 (Data S1, Dataset 1). We established a threshold of 2-fold difference for either SUMO isoform (Figure 5A). Recombinant proteins containing the SIMs from RNF4, a STUbL, have been used previously as traps to purify endogenously sumoylated proteins due to their high affinity for SUMO (Da Silva-Ferrada et al., 2013). Interestingly, we have identified proteins with higher affinities for SUMO2 chains than RNF4 (Figure 5A; Data S1, Dataset 1), including MORC3, TDP2, SETDB1, SLX4, MRE11A, and C18orf25. We searched for *in silico* predicted SIMs in these proteins using the GPS-SUMO tool (Zhao et al., 2014) and synthesized biotinylated peptides containing SIMs in these proteins and mutant counterpart peptides in which long aliphatic residues (I/L/V) had been mutated into alanines. We performed ELISA assays using wells coated with SIM- or mutant SIM-bearing peptides and tested the binding of SUMO2 trimers (Eifler et al., 2018) (Figures 5B and S4A). As a reference, we included peptides corresponding to RNF4 SIMs. SIMs in MORC3 or SETDB1, which have higher affinities for SUMO2 compared to RNF4 (Figure 5A), showed higher binding in the SIM-peptide ELISA assay. The affinity for SUMO2 was abolished in the case of the mutant counterpart peptides.
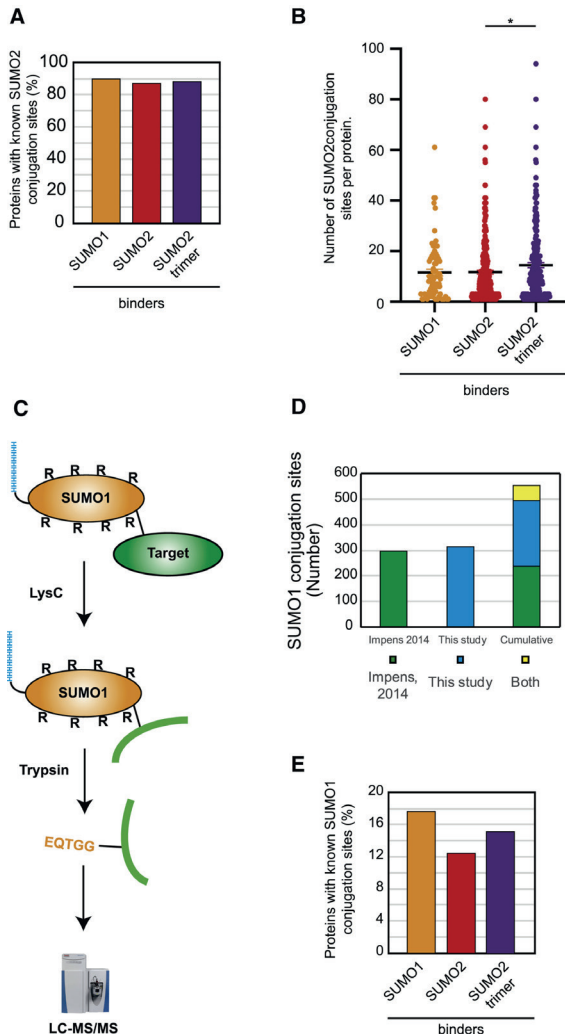
Figure 4. SUMO-binding proteins are also SUMO target proteins. (A) Graph depicting the fraction of SUMO binders for which SUMO2 conjugation sites have been described. **(B)** Graph depicting the number of sumoylation sites identified per protein group in SUMO1, SUMO2, or SUMO2 trimer binders. Each dot represents a protein group. *p < 0.05 Mann-Whitney test. **(C)** Experimental design for identification of SUMO1 conjugation sites. Lysine-deficient HIS-SUMO1-Q92R conjugates were purified from cells, treated with LysC endopeptidase, re-purified, and treated with trypsin. EQTGG remnant-bearing peptides corresponding to SUMO1 conjugation sites were identified by mass spectrometry. **(D)** Graph depicting the number of SUMO1 conjugation sites identified in a previous study (Impens et al., 2014), this study, and the overlap between them. **(E)** Graph depicting the fraction of SUMO1, SUMO2, and SUMO2 trimer binders for which SUMO1 conjugation sites have been identified.

Next, proteins with a preference for SUMO1, SUMO2, or no preference for SUMO isoforms were analyzed to search for predicted SIMs (Data S1, Dataset 9). Next, the predicted SIMs were analyzed by iceLogo (Colaert et al., 2009) to search for putative isoform-specific SIM motifs (Figures 5C and S4B). While amino acids with acidic side chains such as aspartic acid and glutamic acid were overrepresented in the region surrounding the SIMs in proteins with higher affinity for SUMO2, in the SIMs of proteins with higher affinity for SUMO1, lysines and prolines were enriched in close proximity to the SIM. We investigated whether peptides containing corresponding motifs could be used for the generation of more efficient SUMO traps compared to RNF4 SIM-based traps. Biotinylated peptides were synthesized, containing putative SIMs or their respective mutant counterparts, and their affinities for

SUMO2 were evaluated by ELISA (Figures 5D and S4C). First, SUMO2 preferential motif peptides containing multiple acidic residues that are known to contribute to their high affinity for SUMOs (Hecker et al., 2006) had a higher affinity for SUMO2 trimers as compared to RNF4 SIMs. Peptides containing the SUMO1-preferential motif or its mutant counterpart showed no affinity for SUMO2 trimers. Of note, we have been unable to identify a SUMO1 antibody that is functional in ELISA. Second, we tested whether the high-affinity SUMO2 SIM could be used to improve SUMO2 traps. We bound the biotinylated peptides to streptavidin-coated agarose beads, incubated them with cell lysate, washed the beads, and eluted with 8 M urea buffer. Subsequently, we verified the purification efficiency of SUMO2 conjugates by immunoblotting (Figure 5D). Our results indicate that the SUMO-2 preferential trap improved the enrichment of SUMO2 conjugates compared to the RNF4 SIM-based trap.
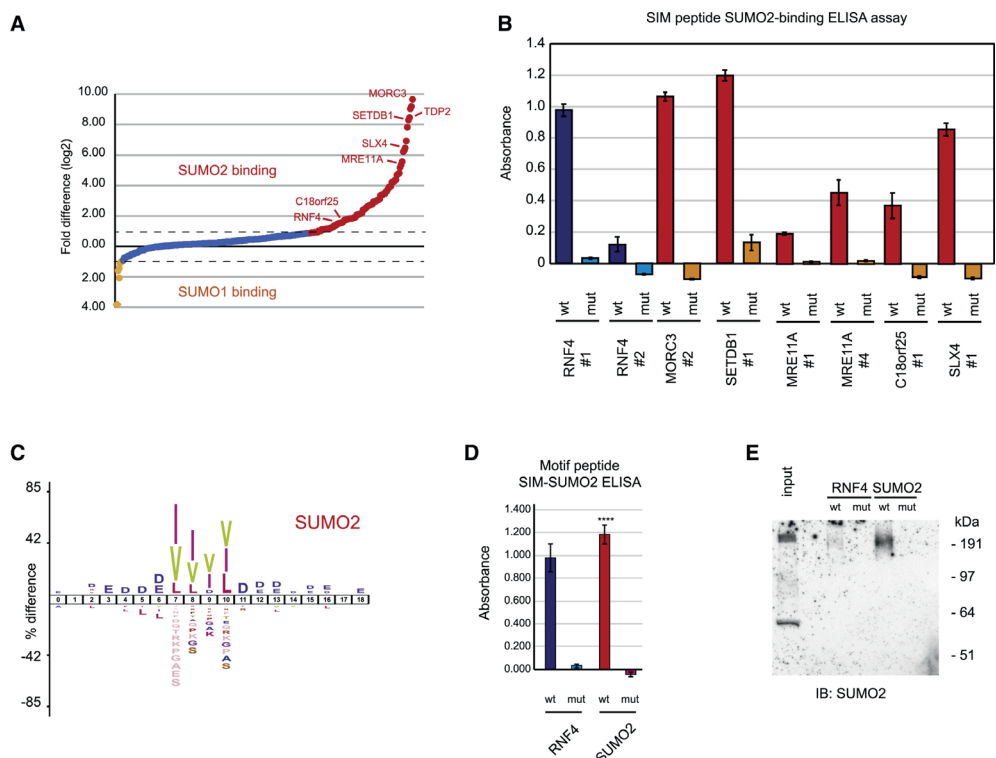

Figure 5. Toward a more efficient SUMO2 trap. (A) SUMO1-SUMO2 differential binding. Average enrichment to control beads of protein groups binding to SUMO1 and/or SUMO2 were compared and a fold-difference (log2) was established and plotted in order from preferential SUMO1 binding toward preferential SUMO2 binding. Each dot represents a protein group. Dotted lines indicate thresholds for preferential SUMO binding. (B) Results from the SUMO2 trimer binding ELISA of selected SIM-containing peptides and controls as indicated. Average and standard deviation from 3 independent experiments in triplicate (n = 9) are shown. (C) IceLogo of predicted SIMs from preferential SUMO2 binders. (D) Results from the SUMO2-trimer ELISA using a peptide containing the preferential SUMO2 SIM motif and controls. Average and standard deviation from 3 independent experiments in triplicate

Figure 5 *(continued)*

(n = 9) are shown. ****p < 0.0001 for a t test. **(E)** Streptavidin beads were coated with peptides containing the indicated SIMs and incubated with cell lysate, washed, and eluted with 8 M urea buffer. SUMO conjugates were analyzed by immunoblotting. The experiment was performed twice.

A SIM in XRCC4 facilitates its recruitment to DNA damage sites

We compared the relative enrichment of the SUMO2 binding proteins with the SUMO2 trimer binding proteins with a cutoff of 2-fold preference (Figure 6A; Data S1, Dataset 1). While protein groups involved in mRNA splicing had higher affinity for SUMO2 polymers, RNA metabolic processes-related protein groups had higher affinity for mono- or multi-SUMO2. Protein groups involved in the DNA damage response and protein sumoylation had similar affinity to SUMO2 and SUMO2 trimer, with the exception of the DNA repair protein XRCC4, which had 7.2 times higher affinity for SUMO2 trimers (Figure 6A). XRCC4 participates in the non-homologous end joining (NHEJ) DNA double-strand break (DSB) repair pathway. Other proteins involved in NHEJ include KU70, KU80, DNA-PKcs, ligase IV, and XLF, among others (Chang et al., 2017; Yang et al., 2016). Interestingly, although XRCC4 was identified as a strong SUMO2 trimer binder, none of the other mentioned NHEJ factors were identified as SUMO-binding proteins (Figure 1B; Data S1, Dataset 1). However, while only 2 SUMO2 conjugation sites have been described for XRCC4, XRCC4 partner proteins in NHEJ KU70, KU80, and DNA-PKcs are extensively sumoylated (Hendriks et al., 2017, 2018). We hypothesized that the SIMs in XRCC4 may be promoting the formation of NHEJ DNA DSB repair complexes via SUMO-SIM interactions.

Sequence analysis of XRCC4 predicted 2 putative SIMs, putative SIM1 in position 33–36 (VITL) and putative SIM2 in position 181–184 (ILVL). Putative SIM1 is located in the Head domain of XRCC4, adjacent to the XLF interacting region, and putative SIM2 is located in the coiled-coil domain, overlapping with the ligase IV-interacting region (Figure 6B). We generated GFP-tagged single and double mutants for these putative SIMs by mutating the long aliphatic residues into alanines and tested their ability to bind SUMO2 trimers (Figure 6C). Mutating putative SIM1 (mut1) reduced the binding of GFP-XRCC4 to the SUMO2 trimer, confirming that it acts as a real SIM, whereas mutating putative SIM2 (mut2) had no effect on SUMO2 trimer binding, indicating that this is not a functional SIM.

SUMO signaling occurs at DNA DSBs (Galanty et al., 2009; Morris et al., 2009), and SIMs in other repair factors such as SLX4 facilitate their recruitment to DNA damage sites (González-Prieto et al., 2015; Ouyang et al., 2015). Therefore, we investigated whether the SIM in XRCC4 was also facilitating its recruitment to local sites of DNA damage. To exclude the possibility that differences in XRCC4 recruitment were due to differences in the recruitment of other components of the NHEJ machinery, the recruitment of KU70 was also monitored as positive

control. U2OS cells were transfected with Ku70-mCherry and constructs encoding either wild-type or SIM mutant GFP-XRCC4. Two days after transfection, DNA damage was induced by multiphoton laser and the recruitment of both constructs was studied in a time-course experiment (Figures 6D and 6E). After laser micro-irradiation, GFP-XRCC4 accumulated at DNA damage sites (Video S1). As hypothesized, removing the SIM significantly reduced the relative recruitment of XRCC4 to the damaged DNA. As an alternative strategy to study the importance of sumoylation for the recruitment of GFP-XRCC4 and Ku70-mCherry to local sites of DNA damage, we treated the cells with SUMO-E1 inhibitor ML-792 at 1 µM (He et al., 2017) for 4 h before laser micro-irradiation experiments, which was sufficient to produce an average reduction of 78% in the amount of SUMO conjugates (Figure S5A). Inhibition of the SUMO E1 enzyme has a similar effect on the recruitment of GFP-XRCC4 to DNA damage tracks compared to the removal of the SIM (Figures 6D and 6E). Interestingly, mutating the SIM in XRCC4 was sufficient to cause a 2-fold increase in the sensitivity to the DSB-inducing agent Bleocin compared to the wild type (Figures 6F and S5B), demonstrating the functional importance of the SIM. Ku70-mCherry was also recruited to DNA damage sites, re-localizing from the nucleoli to the DNA damage sites as previously described (Figures 6D and 6E; Video S2) (Moore et al., 2011). No significant differences were observed in the recruitment of Ku70-mCherry to the local sites of DNA damage induced either by the co-expression of the different GFP-XRCC4 wild-type and SIM mutant constructs or by the inhibition of the SUMO E1 enzyme (Figures 6D and 6E).

Next, we aimed to identify the sumoylated proteins that bind the SIM in XRCC4. To this end, we performed a co-immunoprecipitation experiment with GFP-XRCC4-rescued U2OS XRCC4$^{-/-}$ cells in the presence and absence of Bleocin, and we identified the differentially interacting proteins by mass spectrometry (Figure 7A; Data S1, Dataset 10). We found that the SIM mutant has reduced affinity for ligase IV, and we confirmed this finding by immunoblotting (Figure 7B). Consistently, the stability of ligase IV was decreased in GFP-XRCC4 SIM mutant-rescued XRCC4-deficient cells (Figure 7C). The affinity of other members of the NHEJ complex, including KU70/80 and DNA-PKcs for the agarose beads in negative control samples, was too high to enable the detection of differential affinity between wild-type and SIM mutant GFP-XRCC4 constructs. Nevertheless, XRCC4 phosphorylation on serine 320 in response to Bleocin (Figure S6A) was completely abolished in the SIM mutant (Figure 7D). Interestingly, XRCC4 S320 phosphorylation is mediated by DNA-PKcs (Lee et al., 2004; Sharma et al., 2016; Yu et al., 2003) and this modulates DNA bridging during classical NHEJ (Normanno et al., 2017).
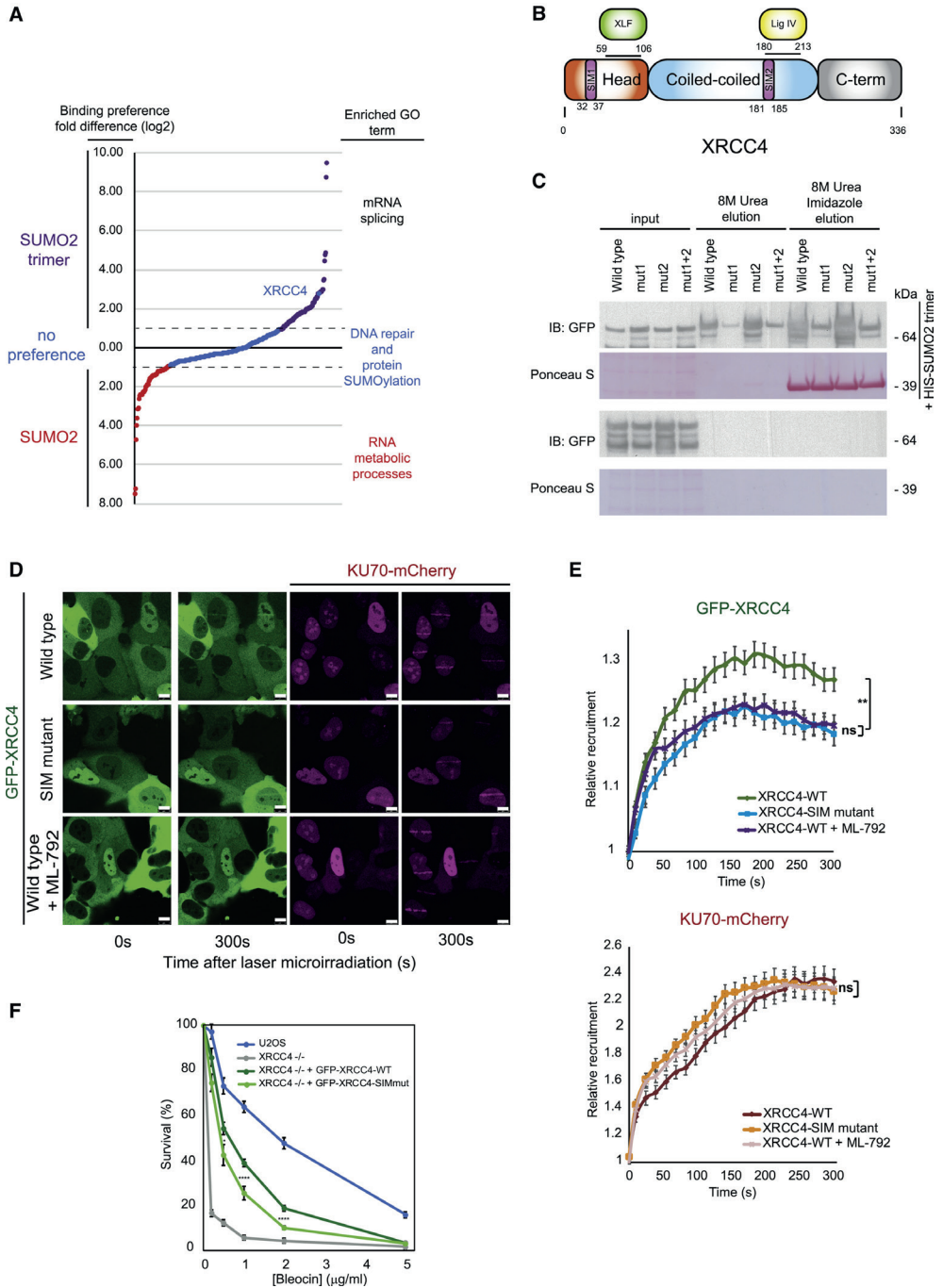
4

Figure 6. A SIM in XRCC4 is important for its recruitment to DNA damage sites.

Figure 6 *(continued)*.

(A) Differential binding of proteins to monomeric or trimeric SUMO2. Protein groups were plotted in order from preferential affinity to SUMO2 toward preferential affinity to SUMO2 trimer. Each dot represents a protein group. Dotted lines indicate thresholds. Gene Ontology terms enriched for the 3 established categories are also indicated. XRCC4 is the only DNA repair protein with higher affinity for SUMO2 trimer than for SUMO2. **(B)** Location of the predicted SIMs within different XRCC4 domains. **(C)** Affinity of different GFP-XRCC4 wild-type and SIM mutant constructs for SUMO2 trimer. Lysates from U2OS cells expressing either GFP-XRCC4 wild-type or SIM mutant constructs were incubated with Ni-NTA beads coated or not coated with HIS-SUMO2 trimer, washed, and eluted. The amount of GFP-XRCC4 bound to the beads was investigated by immunoblotting. The experiment was performed 3 times. **(D)** Laser micro-irradiation experiments in U2OS cells expressing Ku70-mCherry and different GFP-XRCC4 wild-type or SIM mutant constructs. After DNA damage infliction, relative recruitment to the DNA damage sites was investigated in time course experiments. Furthermore, U2OS cells expressing wild-type GFP-XRCC4 were treated with 1 μM ML-792 before micro-irradiation experiments. Scale bars represent 10 μm. **(E)** Quantification of the relative recruitment of GFP-XRCC4 and Ku70-mCherry to the DNA damage sites from **(D)**. Curves represent mean relative recruitment and error bars represent the SEM of values from at least 3 independent experiments (N_{WT} = 74, $N_{SIM\ mut}$ = 73, $N_{wt+ML-792}$ = 91). Kruskal-Wallis tests were performed to determine statistical differences using the area under the curve (AUC) (*$p < 0.05$; **$p < 0.01$; ***$p < 0.001$; ****$p < 0.0001$). **(F)** Result of clonogenic assay to measure cellular sensitivity to the DSB-inducing agent Bleocin in U2OS cells and U2OS XRCC4$^{-/-}$ cells rescued with GFP-XRCC4 wild type or GFP-XRCC4 SIM mutant. Average and SEM of 3 different experiments is indicated ($N_{U2OS,\ XRCC4-WT,\ XRCC4-SIM\ mut}$ = 15; $N_{XRCC4-/-}$ = 10). *$p < 0.05$; **$p < 0.01$; ***$p < 0.001$; ****$p < 0.0001$ for t tests.

We conclude that the formation of the classical NHEJ DNA repair complex is facilitated and stabilized via SUMO-SIM interactions (Figure 7E). Consistent with this model, mutating positions 181–184 (ILVL) of XRCC4 into alanines (LigIV mutant), which abrogated the interaction of XRCC4 with ligase IV (Figure S6B), thus destabilizing the NHEJ complex by hampering end bridging (Ochi et al., 2014), reduced the recruitment or retention of XRCC4 at local sites of DNA damage induced by laser micro-irradiation. Mutating both the SIM and the ligase IV interaction domain had an additive effect (Figure S6C), which suggests that SUMO and ligase IV modulate DNA bridging and NHEJ stability at damage sites in a cooperative manner.

Mutations in XRCC4 are associated with microcephalic primordial dwarfism (Guo et al., 2015; Murray et al., 2015). A missense mutation (W43R) is located close to the SIM and is also associated with the destabilization of ligase IV. We investigated whether this mutation affects SUMO-binding of XRCC4. Therefore, we tested the affinity of GFP-XRCC4-W43R for SUMO2 trimers (Figure S6D). The XRCC4-W43R mutation strongly reduced the SUMO binding of XRCC4 to the same extent as the classical SIM mutant. Thus, the W43R missense mutation of XRCC4, causing microcephalic primordial dwarfism, could be related to reduced SUMO binding.
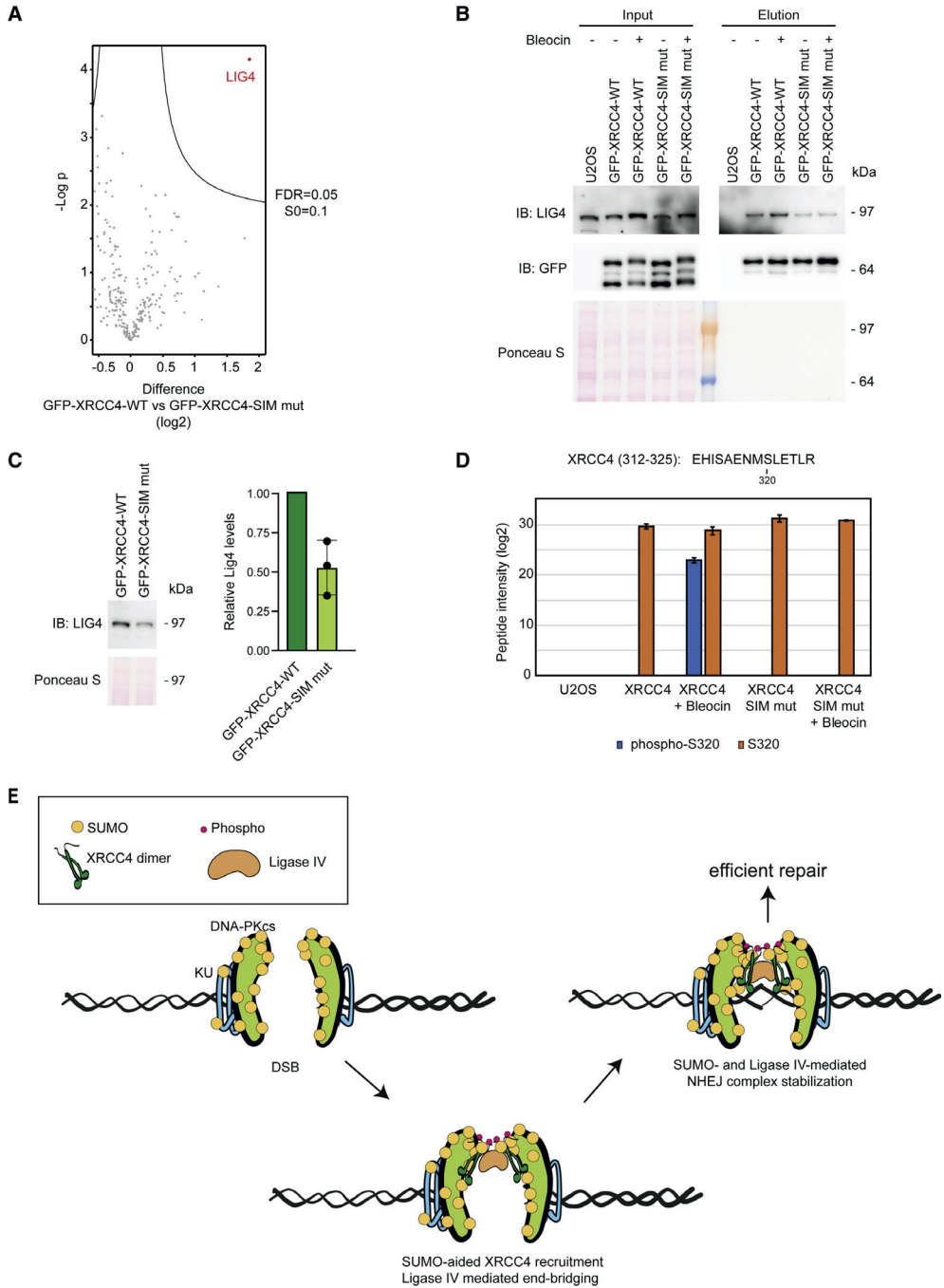
Figure 7. Sumoylation affects the stability of the classic NHEJ complex.

Figure 7 *(continued).*
(A) Volcano plot depicting differential interactors of GFP-XRCC4 wild-type compared to GFP-XRCC4 SIM mutant in U2OS XRCC4$^{-/-}$ cells. The threshold corresponds to permutation-based FDR = 0.05 and S0 = 0.1 from 4 independent experiments. **(B)** Verification by immunoblotting of the results in (A). The experiment was performed 3 times. **(C)** Relative ligase IV levels in U2OS XRCC4$^{-/-}$ cells complemented either with wild-type or SIM mutant constructs of GFP-XRCC4. Average and standard deviation from 3 independent experiments is shown. **(D)** Peptide intensity of the tryptic XRCC4 peptide EHISAENMSLETLR, phosphorylated or not phosphorylated at serine 320 in the different conditions analyzed by mass spectrometry. Average intensity and standard deviation from 3 replicates are shown. **(E)** Speculative model. Sumoylation of the DNA-PK complex at DNA DSBs promotes the recruitment and phosphorylation of XRCC4 on S320. SUMO-SIM interactions enhance the stability of the complex for efficient DSB repair.

DISCUSSION

Different SUMO isoform binders

Here, we have investigated proteins that bind SUMO family members in a non-covalent manner. SUMO1 and SUMO2/3 differ 53% in their amino acid sequence. Nevertheless, they share the same protein structure and enzymatic machinery. SUMO2/3 is the most abundant isoform in human cells (Saitoh and Hinchey, 2000). Interestingly, while 298 of the 379 SUMO-binding proteins do not bind to SUMO1, only 9 of 379 are exclusive SUMO1 binders (Figure 1C). This implies that non-covalent binding is more selective for signal transduction in the case of SUMO1 compared to SUMO2.

Interestingly, SUMO2 trimer-binding proteins are covalently sumoylated to a higher degree compared to SUMO2 monomer-binding proteins (Figure 4B), supporting the idea of a feedforward mechanism in the stabilization of protein complexes via SUMO-SIM interaction, as previously described (Psakhye and Jentsch, 2012). Moreover, poly-sumoylation may determine protein fate by enabling the participation of a protein in different protein complexes, depending on its sumoylation levels and SUMO chain extension state.

Compared to previous studies aiming to identify SUMO interactors in a proteome wide manner (Aguilar-Martinez et al., 2015; Cox et al., 2017; Hecker et al., 2006; Ouyang et al., 2009) and compared to 44 proteins independently described in the literature to interact with SUMO (Aguilar-Martinez et al., 2015; Anamika and Spyracopoulos, 2016; Arriagada et al., 2011; Cappadocia et al., 2015; Cho et al., 2009, 2013; Cong et al., 2011; Danielsen et al., 2012; de la Cruz-Herrera et al., 2017; Diehl et al., 2016; Du et al., 2010; Eisenhardt et al., 2015; Escobar-Cabrera et al., 2011; Garzón et al., 2011; Guervilly et al., 2015; Guzzo et al., 2014; Hickey et al., 2012; Hwang and Lee, 2017; Kaur et al., 2017; Lecona et al., 2016; Li et al., 2017; McLaughlin et al., 2016; Meng et al., 2016; Merrill et al., 2010; Meulmeester et al., 2008; Ouyang et al., 2009; Saether et al., 2011; Sahoo et al., 2017; Santiago et al.,

2009; Schellenberg et al., 2017; Seenivasan et al., 2019; Sekiyama et al., 2008; Sridharan and Azuma, 2016; Sriramachandran et al., 2019; Sun et al., 2014; Sung et al., 2011; Tapia et al., 2014; Tatham et al., 2008; Wang et al., 2019; Zhang et al., 2008, 2019), 302 of the 379 proteins identified in our study have not been described before to interact with SUMO (79.7%) (Figure S7; Data S1, Dataset 11). From the group of 44 proteins independently described in the literature to interact with SUMO, including SUMO ligases, SUMO proteases, and STUbLs, we identified 20 proteins in our study; 18 of these proteins are significantly enriched compared to control samples, which is an indication of the high coverage of the SUMO interactor proteome we have reached in our study. This number is considerably higher compared to other previously published proteome-wide SUMO interaction studies: Ouyang et al. (2009) (11 of 44), Aguilar-Martinez et al. (2015) (8 of 44), Hecker et al. (2006) (6 of 44), or Cox et al. (2017) (1 of 44) (Data S1, Dataset 10). Furthermore, in our study, the affinity for the different SUMO family members of each protein was measured in a quantitative manner, while previous studies were performed in a qualitative manner. Twenty of the 44 proteins independently described in the literature to interact with SUMO have not been identified in any of the proteome-wide screens, which could be due to cell line-specific protein expression as well as to the technical limitations of the methods used in the different studies.

XRCC4 contains a functional SIM

Among the SUMO2-binding proteins, XRCC4 has a higher affinity for SUMO2 trimers than for mono-SUMO2. Interestingly, mutating a single SIM in XRCC4 abolished its interaction with SUMO2 trimers. This can be explained by XRCC4's acting as a dimer to form a complex with ligase IV (Sibanda et al., 2001). Furthermore, XRCC4 forms long polymeric structures with XLF (Ochi et al., 2014). Thus, mutating a single SIM in XRCC4 leads to a loss of two SIMs in the XRCC4 dimer and potentially more SIMs upon polymerization with XLF, which is consistent with a loss of SUMO polymer binding.

Abolishing the interaction of XRCC4 with SUMO2 had the same effect on recruitment kinetics to local sites of DNA damage as inhibiting the SUMO E1 enzyme (Figures 6D, 6E, and S5). Mutating the SIM reduced the affinity of XRCC4 for ligase IV and consequently reduced the stability of ligase IV (Figures 7A–7C). Unlike other members of the classical NHEJ complex, sumoylation of ligase IV has not been described at endogenous levels (Hendriks et al., 2018), and ligase IV and SUMO stabilize XRCC4 at local sites of DNA damage in a cooperative manner (Figure S6C). The high affinity of the DNA-PK complex (KU70/80 and DNA-PKcs) as a background binder hampered detecting differential affinities between wild type and SIM mutant GFP-XRCC4 constructs by MS analysis. However, XRCC4 S320 phosphorylation

in response to DNA damage, which is mediated by DNA-PKcs (Lee et al., 2004; Sharma et al., 2016; Yu et al., 2003), was completely abolished in the SIM mutant (Figure 7D). This piece of evidence, combined with high endogenous sumoylation levels of KU70, KU80, and DNA-PKcs, with 23, 19, and 9 sites, respectively (Hendriks et al., 2018), indicates a role for sumoylation of the DNA-PK complex members in recruiting XRCC4 via its SIM.

Functionally, mutating the SIM in XRCC4 was sufficient to reduce cellular resistance to the DSB-inducing agent Bleocin by 2-fold compared to the wild-type counterpart (Figure 6E). This is in agreement with our expectations, as mutating a single SIM is unlikely to completely abolish the functionality of the highly SUMO-regulated NHEJ repair complex (Psakhye and Jentsch, 2012). Effects in survival assays for other previously described SIM mutants have been milder (González-Prieto et al., 2015; Guervilly et al., 2015; Ouyang et al., 2015). This is in line with the concept of functional protein group regulation proposed by Stefan Jentsch (Psakhye and Jentsch, 2012).

Future perspectives

The results obtained in this project lead to additional research questions that could be further investigated. Surprisingly, we could not identify the nuclear pore complex subunit RanBP2 as a SUMO1-binding protein. RanBP2 is known to interact with the most important exclusive SUMO1 target RANGAP1 (Mahajan et al., 1997, 1998; Matunis et al., 1996, 1998; Vertegaal et al., 2006). This indicates that our screen is not exhaustive, and many more proteins may interact with SUMO only in the proper context of the relevant covalent target proteins. Moreover, our set-up may be suboptimal for proteins interacting with nuclear membranes. Concerning SIM motifs, SIMs in proteins such as MORC3 or SETDB1 have a higher affinity for SUMO2 compared to RNF4 (Figure 5A; Data S1, Dataset 1). Consistently, high SUMO2 affinity SIMs in MORC3 and SETDB1 contain acidic stretches adjacent to the long aliphatic residues, which is consistent with the high-affinity SUMO2 consensus SIM (Figure 5C). Furthermore, we noted that whereas TDP2 is a very strong SUMO binder in our screen, the corresponding SIM peptides did not bind to SUMO. This is consistent with the notion that TDP2 binds to SUMO2 via a split SIM (Schellenberg et al., 2017). These results indicate that the split SIM in TDP2 may be a very-high-affinity SUMO2-binding motif. Other proteins with high affinities for SUMO2 in our screen also lack acidic stretch-surrounded SIM motifs (e.g., ARL14EP, ATF7IP), which may be an indication that they also contain split SIMs. Furthermore, detailed investigation of the functional relevance of non-covalent SUMO interaction for the identified set of proteins represents a considerable challenge.

EXPERIMENTAL MODEL AND SUBJECT DETAILS

U2OS, HeLa, HT-1080 and HEK293T cell lines listed in the Key resources table were cultured in DMEM high glucose medium supplemented with 10% FBS and 100 U/mL penicillin plus 100 μg/mL streptomycin (Thermo-Fisher) at 37°C at 5% CO_2.

METHODS

Plasmids construction

GFP-XRCC4 SIM mutants were constructed by site-directed mutagenesis using oligos: FW-SIM1: 5'-GGAATCTGGTTTTGCTGCTACAGCTACTGATGGTCATTC- 3', RV-SIM1: 5'-GAATGACCATCAGTAGCTGTAGCAGCAAAACCAGATTCC- 3', FW-SIM2: 5'-CTTTATAAGCGGTTTGCTGCGGCGGCGAATGAGAAGAAAAC- 3', RV-SIM2: 5'-GTTTTCTTCTCATTCGCCGCCGCAGCAAACCGCTTATAAAG- 3'. Mutants were generated in ENTRY clone pENTR221 and transferred by Gateway cloning to pDEST-EGFP-myc. This plasmid was produced by cloning EGFP in between the NdeI and HindIII sites of pDEST-myc, a kind gift of Dr. Simon Boulton (Martin et al., 2005). GFP-XRCC4 W43R was constructed using site-directed mutagenesis using oligos: FW-W43R: 5'-CACTTACTGATGGTCATTCAGCAAGGACTGGGACAGTTTCTGAATC-3' and RV-W43R: 5'-GATTCAGAAACTGTCCCAGTCCTTGCTGAATGACCATCAGTAAGTG-3'. This mutant was generated directly in pDEST-EGFP-myc. KU70-mCherry was constructed by Gateway cloning using clone ccsbBroadEn_00604 from the Human ORFeome library into pDest-mCherry-N1. pDest-mCherry-N1 was a kind gift from Dr. Robin Shaw (Hong et al., 2010). GFP-XRCC4 wild-type and SIM mutant were amplified by PCR using oligos BP-FW-eGFP: 5'-GGGGACAAGTTTGTACAAAAAAGCAGGCTTCATGGTGAGCAAGGGCGAG-3' and BP-RV-XRCC4: 5'-GGGGACCACTTTGTACAAGAAAGCTGGGTaAATCTCATCAAAGAGGTCTTCTGGG-3' and transferred by a BP-Gateway reaction into pDONR207 and then transferred by a Gateway LR reaction into pLX303, which was a gift from David Root (Addgene plasmid # 25897) (Yang et al., 2011).

Antibodies

Primary antibodies used in this study are the following: mouse-anti-SUMO2/3 (8A2, obtained from Developmental Studies Hybridoma Bank (DSHB), University of Iowa, in-house produced), mouse-anti-XRCC4 (Signalway antibody, 40455), rabbit-anti-PTRF (Bethyl, A301-269), rabbit-anti-ERCC1 (Cell Signaling Technology, 12345T), rabbit-anti-ARKL1 (Bethyl, A303-393), rabbit-anti-RNF216 (Bethyl, A304-111), rabbit-anti-ATRX (Bethyl, A301-045), rabbit-anti-BLM (Abcam, ab476-100), rabbit-anti-GFP (Novus Biologicals, NB600-308),

rabbit-anti-DNA Ligase IV (Cell Signaling Technology, 14649).

Cell culture and cell lines

U2OS cells and HeLa cells were grown in DMEM high glucose medium supplemented with 10% FBS and 100 U/mL penicillin plus 100 µg/mL streptomycin (Thermo-Fisher) at 37°C at 5% CO2. Cells were regularly tested for mycoplasm contamination and found to be negative· U2OS XRCC4$^{-/-}$ cells were a kind gift from Dr· Haico van Attikum in our institute (Singh et al. under review). GFP-XRCC4 rescued cell lines were generated by lentiviral transduction with pLX303-GFP-XRCC4 and pLX303-GFP-XRCC4-SIM mutant. Next, they were sorted for GFP intensity in a FACS Aria and the lowest 1% intense GFP-positive cells were selected.

Recombinant HIS-SUMO1, HIS-SUMO2, HIS-SUMO2 trimer production

SUMO isotypes for the SUMO binders screen were produced as described in Eifler et al. (2018). 10HIS-tagged SUMO1, SUMO2 or SUMO2 trimer, all three lacking the -GG terminal motif, were recombinantly expressed in BL21 cells by inducing protein expression at an O.D.$_{600}$ of 0·6 with 0.5 mM IPTG and incubated overnight at 25°C· Cells were lysed in 50 mM HEPES pH7·6, 0.5 M NaCl, 25 mM MgCl$_2$, 20% glycerol, 0.1% N-P40, 50 mM imidazole, 1 mM phenylmethanesulfonylfluoride (PMSF), and protease inhibitor cocktail minus EDTA (Roche), and the HIS-SUMO constructs were purified from lysates by incubating with Ni-NTA beads (QIAGEN) for 3 h at 4°C. Beads were then washed twice in lysis buffer including PMSF and protease inhibitor cocktail (Roche, 11836170001) and twice in lysis buffer without PMSF and protease inhibitor cocktail. Proteins were eluted by incubating with lysis buffer plus 500 mM imidazole for 10 min at 4°C. The elution step was repeated three times.

SUMO binders sample preparation

400 µL Ni-NTA bead slurry was washed three times with wash buffer (50 mM Tris pH7.5, 150 mM NaCl, 0.5% NP-40, 50 mM imidazole) and split over 4 tubes. To three of them, 100 µg of recombinant HIS-SUMO1, HIS-SUMO2 or HIS-SUMO2 trimer was added. The last aliquot of beads was used as negative control. Beads were incubated with the different HIS-SUMO isotypes for 2 hr at 4°C while rotating and then washed again 3 times with wash buffer.

Twenty confluent 15 cm dishes of HeLa cells were lysed in 4 mL of lysis buffer (50 mM Tris pH7.5, 150 mM NaCl, 0.5% NP-40, 50 mM imidazole, Protease Inhibitor Mix without EDTA (Roche, 11836170001), sonicated 2 times for 10 s, split over 1.5 mL microcentrifuge tubes and centrifuged 1 hr at 4°C at 16,000 x g. Supernatants were pooled and input control

sample was taken. A quarter of the supernatant was added to each of the tubes containing the bead-bound SUMO isotypes or beads only and incubated 2 hr at 4°C. Unbound control samples were also taken.

After incubation, beads were washed 3 times for 10 min with 500 µL of wash buffer, including one tube change. Subsequently, they were washed 3 times for 10 min with 500 µL 50 mM Tris pH7.5, 150 mM NaCl, including one tube change. The first elution was performed with 100 µL 8 M urea, 50 mM Tris pH7.5 for 30 min at room temperature. The second elution was performed with 100 µL 8 M urea, 50 mM Tris pH7.5, 500 mM imidazole for 30 min at room temperature. Elutions were transferred to a pre-washed 0.45 µm filter column (Millipore), and centrifuged at 10,000 x g to separate the elution from the remaining beads. A small part of the elution was kept for immunoblotting.

Samples from the first elution were concentrated by passing through a 5 kDa cut-off filter prewashed with elution buffer 1. Concentration was performed by centrifugation at 8,000 x g at room temperature in a temperature-controlled centrifuge. Next, the proteins were washed once with 250 µL elution buffer. Concentrated sample-volumes were equalized at 25 µL using elution buffer 1. Ammonium bicarbonate (ABC) was added to a final concentration of 50 mM from a 1 M stock. Dithiothreitol (DTT) was added to a final concentration of 1 mM, and incubated for 30 min at room temperature, followed by adding 5 mM chloroacetamide (CAA) for 30 min at room temperature, and 5 mM extra DTT for 30 min at room temperature. Next samples were diluted 4-fold with 50 mM ABC, and 500 ng of Trypsin (V5111, Promega) was added. Trypsinization was performed overnight, still and in the dark.

SUMO-binding capacity of XRCC4 mutants

SUMO2 trimer-binding capacity of the different GFP-XRCC4 constructs was assayed by using the aforementioned SUMO binders enrichment protocol using cell lysates from cells transfected with the different GFP-XRCC4 plasmids.

SUMO1 conjugation sites sample preparation

Ten confluent 15 cm dishes of HT-1080 cells expressing lysine-deficient HIS-SUMO1-Q92R were treated as previously described (Hendriks et al., 2014). In brief, cells were washed three times on the dish with ice-cold PBS before being scraped and collected. Subsequently, the cell pellets were lysed in 10 pellet volumes of guanidine lysis buffer (6 M guanidine-HCl, 100 mM sodium phosphate, and 10 mM Tris, buffered at pH 8.0) and sonicated. Next, lysates were supplemented with imidazole to 50 mM and β-mercaptoethanol to 5 mM. 20 µL (dry volume) of pre-washed Ni-NTA agarose beads (QIAGEN) were added per 1 mL

lysate and incubated overnight at 4°C while rotating. Next, beads were washed for at least 15 min with at least five bead volumes of the following wash buffers in order: wash buffer 1 (6 M guanidine-HCl, 0.1% Triton X-100, 10 mM imidazole, 5 mM β-mercaptoethanol, 100 mM sodium phosphate, and 10 mM Tris, pH 8.0), wash buffer 2 (8 M urea, 0.1% Triton X-100, 10 mM imidazole, 5 mM β-mercaptoethanol, 100 mM sodium phosphate, 10 mM Tris, pH 8.0), wash buffer 3 (8 M urea, 10 mM imidazole, 5 mM β-mercaptoethanol, 100 mM sodium phosphate, 10 mM Tris, pH 6.3), wash buffer 4 (8 M urea, 5 mM β-mercaptoethanol, 100 mM sodium phosphate, 10 mM Tris, pH 6.3), two times. Subsequently, all wash buffer was removed from the beads, and proteins were eluted for 30 min with one bead volume of elution buffer (7 M urea, 500 mM imidazole, 100 mM sodium phosphate, and 10 mM Tris, buffered at pH 7.0). The elution procedure was repeated another two times, and all eluates were pooled and passed through 0.45-µM filters (Ultrafree, Millipore). Finally, samples were concentrated over 100 kDa cut-off filters (Vivacon 500, Sartorius Stedim) at 20°C and at 8,000 x g until 10–50 µL of sample remained.

After concentration, the proteins remaining on the filters were washed once with 250 µL of elution buffer minus imidazole and re-concentrated. Final concentrated sumoylated proteins were removed from the filters and sequencing-grade endoproteinase Lys-C (Wako) was added to the samples in a 1:25 enzyme/protein ratio and incubated for 4 h at room temperature, still and in the dark. Subsequently, another 10 mM of fresh β-mercapto-ethanol was added to the samples, and this was followed by an additional amount of Lys-C equal to the first amount. The second incubation was performed overnight, at room temperature, still and in the dark. Next, digests were transferred to 15-mL tubes and diluted with an amount of guanidinium lysis buffer equal to half the amount used to lyse the initial cell pellet. The samples were then supplemented with imidazole to 50 mM and β-mercapto-ethanol to 5 mM. Next, 40 µL (dry volume) Ni-NTA agarose beads (QIAGEN) were prepared per 1 mL sample. The equilibrated beads were added to the lysates and allowed to tumble at 4°C for 5 h and washes and elutions were repeated as described for the first purification. Next, samples were concentrated on 10 kDa cut-off spin filters (Vivacon 500, Sartorius Stedim) at 20°C and at 14,000 x g. Concentration was performed until 10–25 µL of sample remained. After concentration, the proteins remaining on the filters were washed twice with 250 µL of elution buffer minus imidazole and re-concentrated. Final concentrated sumoylated peptides were removed from the filters.

SUMO1 conjugated peptides were supplemented with ABC to 50 mM from a 1 M stock. DTT was added to a final concentration of 1 mM, and incubated 30 min at room temperature, followed by 5 mM Chloroacetamide (CAA) for 30 min at room temperature, and 5 mM extra DTT for 30 min at room temperature. Next samples were diluted 4 fold with 50 mM ABC

and an amount of sequencing-grade modified trypsin (V5111, Promega) was added equal to 25% of the Lys-C initially used in a single digestion step. Digestion was performed overnight, at room temperature, still and in the dark.

Sample preparation of GFP-XRCC4 interactors

U2OS XRCC4$^{-/-}$ complemented with either wild-type or SIM mutant constructs of GFP-XRCC4 were treated or not with 5 µg/mL Bleocin (Millipore) for two hours. Upon confluency, cells were scraped, washed in ice-cold PBS and lysed in 1 mL of ice-cold lysis buffer (20 mM Tris pH 7.5, 150 mM NaCl, 1 mM MgCl$_2$, 0.5% Triton X-100, protease inhibitors minus EDTA (Roche), 20 mM N-Ethylmaleimide (NEM)). Lysates were vortexed and incubated 1 hr at 4°C while rotating after adding 500 Units of Benzonase (Millipore) per sample. Subsequently, samples were centrifuged for 1 hr at 20,000 x g and 4°C and supernatants were incubated with 50 µL of GFP-Trap beads slurry (Chromotek) for 90 min at 4°C while rotating. Subsequently, beads were washed twice with 1 mL of wash buffer (20 mM Tris pH 7.5, 150 mM NaCl, 1 mM MgCl$_2$, protease inhibitors minus EDTA (Roche), 20 mM NEM) and 5 times with 1 mL 50 mM ABC. Finally, beads were resuspended in 250 µL of 50 mM ABC and 500 ng of Trypsin (V5111, Promega) was added and samples were incubated overnight at 37°C while shaking at 1,400 rpm. Digested peptides were separated from the beads by passing through a pre-washed 0.45 µm filter (Millipore).

Stage-tipping

Prior to LC-MS/MS analysis, all trypsin-digested peptide solutions were desalted and concentrated on STAGE-tips as described previously (Rappsilber et al., 2007) and eluted with 80% acetonitrile in 0.1% formic acid or 60% acetonitrile in 0.1% formic acid for the GFP-XRCC4 samples. Elutions were vacuum dried, employing a SpeedVac RC10.10 (Jouan, France), and dissolved in 10 µl 0.1% formic acid before online nanoflow liquid chromatography-tandem mass spectrometry (nanoLC-MS/MS).

Mass spectrometry data acquisition

All the experiments were performed on an EASY-nLC 1000 system (Proxeon, Odense, Denmark) connected to a Q-Exactive Orbitrap (Thermo Fisher Scientific, Germany) through a nano-electrospray ion source. The Q-Exactive was coupled to a 15 cm analytical column with an inner-diameter of 75 µm, in-house packed with 1.9 µm C18-AQ beads (Reprospher-DE, Pur, Dr. Manish, Ammerbuch-Entringen, Germany). The chromatography gradients were from 2% to 95% acetonitrile in 0.1% formic acid at a flow rate of 200 nL/min and the mass spectrometer was operated in a Data-Dependent Acquisition (DDA) mode. Different

gradient lengths and MS1 and MS2 settings are specified.

For the SUMO-binder screen, the gradient length was 60 min with a top-10 method and a scan range of 400-2000 m/z. Full-scan MS spectra were acquired at a target value of 3×10^6 and a resolution of 70,000, and the Higher-Collisional Dissociation (HCD) tandem mass spectra (MS/MS) were recorded at a target value of 1×10^5 and with a resolution of 17,500, and isolation window of 2·2 m/z, and a normalized collision energy (NCE) of 25%. The minimum AGC target was 1×10^3. The maximum MS1 and MS2 injection times were 20 and 60 ms, respectively. Two technical repeats were performed per sample. The precursor ion masses of scanned ions were dynamically excluded (DE) from MS/MS analysis for 60 s. Ions with charge 1, and > 6, were excluded from triggering MS2 analysis.

For the SUMO1 sites identification, the gradient length was 125 min with a top-5 method and a scan range of 300-1750 m/z. Full-scan MS spectra were acquired at a target value of 3×10^6 and a resolution of 70,000, and the HCD-MS/MS spectra were recorded at a target value of 1×10^5 and with a resolution of 17,500, an isolation window of 1·6 m/z, and a NCE of 25%. The minimum AGC target was 2×10^2. The maximum MS1 and MS2 injection times were 20 ms and 250 ms, respectively. Samples were analyzed in technical triplicates. The precursor ion masses of scanned ions were dynamically excluded (DE) from MS/MS analysis for 60 s. Ions with charge 1, and > 6, were excluded from triggering MS2 analysis.

For the GFP-XRCC4 interactor screen, the gradient length was 90 min with a top-7 method and a scan range of 300-1600 m/z. Full-scan MS spectra were acquired at a target value of 3×10^6 and a resolution of 70,000, and HCD-MS/MS spectra were recorded at a target value of 1×10^5 and with a resolution of 35,000, and isolation window of 2·2 m/z, and a NCE of 25%. The minimum AGC target was 1×10^4. The maximum MS1 and MS2 injection times were 250 ms and 120 ms, respectively. The precursor ion masses of scanned ions were dynamically excluded (DE) from MS/MS analysis for 20 s. Ions with charge 1, and > 6, were excluded from triggering MS2 analysis.

Mass spectrometry data analysis

All raw data were analyzed using MaxQuant (version 1.6.3.3) as described previously (Tyanova et al., 2016a). We performed the search against an *in silico* digested UniProt reference proteome for *Homo sapiens* including canonical and isoform sequences (30th November 2018), or a canonical only in the case of the SUMO1 sites (18th April 2019).

Database searches were performed according to standard settings with the following modifications for the different datasets.

For the SUMO binders, digestion with Trypsin/P was used, allowing 4 missed cleavages. Oxidation (M) and Acetyl (Protein N-term) were allowed as variable modifications with a maximum number of 3. Carbamidomethyl (C) was disabled as a fixed modification. Label-Free Quantification was enabled, not allowing Fast LFQ. Match between runs was performed with 0.7 min match time window and 20 min alignment time window. All peptides were used for protein quantification. All tables were written.

For the SUMO1 sites, digestion with Trypsin/P was used, allowing 4 missed cleavages. Oxidation (M) and Acetyl (Protein N-term), EQTGG (K) and Phospho (ST) were allowed as variable modifications with a maximum number of 5. Carbamidomethyl (C) was set as a fixed modification. Label-Free Quantification was disabled. All peptides were used for protein quantification. All tables were written.

For the GFP-XRCC4 interactors, digestion with Trypsin/P, allowing 3 missed cleavages. Oxidation (M) and Acetyl (Protein N-term), and Phospho (ST) were allowed as variable modifications with a maximum number of 3. Carbamidomethyl (C) was disabled as a fixed modification and NEM (C) enabled. Label-Free Quantification was enabled, not allowing Fast LFQ. Match between runs was performed with 0.7 min match time window and 20 min alignment time window. All peptides were used for protein quantification. All tables were written.

Laser micro-irradiation experiments

Approximately 20,000 U2OS cells were seeded in six-well dishes containing an 18 mm coverslip. The following day, GFP- and mCherry-tagged protein construct plasmids were co-transfected in tandem using 1 µg of DNA per plasmid (2 µg in total) and 12 µl of PEI (1 mg/mL) for 24 hr. Subsequently, medium was replaced with fresh medium.

Laser micro-irradiation experiments were performed two days after transfection as in González-Prieto et al. (2015). In brief, experiments were performed using a Leica SP5 confocal microscope with an environmental chamber set to 37°C. Two days after transfection, media was replaced by CO_2-independent Leibovitz's L15 medium supplemented with 10% FCS and pen/strep. DNA damage tracks of 1 µm width were generated with a Mira mode-locked titanium-sapphire (Ti:Sapphire) laser (I = 800 nm, pulse length = 200 fs, repetition rate = 76 MHz, output power = 80 mW) using a UV-transmitting 63× 1.4 NA oil immersion objective (HCX PL APO; Leica). Confocal images were recorded before and after laser irradiation at 15 s time intervals over a period of 5 min. Images were analyzed using Leica LAS AF software. For statistical analysis of differences in the recruitment, non-parametric Mann-Whitney's or Kruskal-Wallis tests using the Area Under the Curve (AUC) were used.

Clonogenic survival assays

Three thousand cells per well were plated in 6-well plates and allowed to attach overnight before treatment. Bleocin (Millipore) was added for 6 hours at different concentrations, after which medium was replaced for fresh DMEM. Subsequently, cells were allowed to grow for 10 days and fixed for 5 minutes in paraformaldehyde 4% in PBS. Cells were stained with Crystal Violet 0.05% for 30 minutes and washed 3 times with water. Afterward, Crystal Violet was re-solubilized in methanol and O.D.$_{595}$ was measured. The value of untreated cells was set at 100%.

SIM-peptide binding assay

The SIM-peptide binding assays were performed as described in Eifler et al. (2018). In brief, peptides were synthesized on a SYRO II synthesizer, using preloaded Wang resin and standard Fmoc Solid Phase Peptide Chemistry, with PyBop and Dipea as activator and base. For the binding assay, wells of Streptavidin High Capacity Coated Plates (Sigma, 96-well, clear, S6940) were pre-washed three times with 200 µL 1 × PBS per well. Peptides were added to the wells overnight at 4°C at a concentration of 500 pmol per mL. Subsequently, blocking solution (0.4% BSA in PBS) was added for 30 min at room temperature and the wells were washed three times with 200 µL 1 × PBS/0.05%Tween 20. The wells were incubated with 50 µL of recombinant SUMO2 trimer at 10 µg per mL for 90 min at 4°C. Unbound protein was removed by washing three times with 200 µL PBS/0.05%Tween 20 and 50 µL of SUMO2/3 mouse monoclonal antibody 8A2 (dilution 1:48) was added and incubated for 90 min at 4°C. Wells were washed another three times with 200 µL PBS/0.05%Tween 20 and 50 µL of horseradish peroxidase-coupled anti-mouse secondary antibody (dilution 1:200) was added and incubated for 90 min at 4°C. Unbound antibody was removed by washing three times with 200 µL PBS/0.05%Tween 20 and 100 ul of a 1:1 dilution of the reagents A and B in the Color Reagent Pack (R&D Systems) was added to the wells. The plate was incubated at room temperature in the dark until the positive controls were colored and the reaction was stopped with 50 µL 1 M H_2SO_4 per well. Binding of the peptides was determined by measuring the absorbance at 450 nm in a plate reader (Perkin Elmer Victor X3).

Quantification and statistical analysis

For the statistical analysis of mass spectrometry data, output from the analysis in MaxQuant from the SUMO binders was further processed in the Perseus computational platform (v 1.6.2.2) (Tyanova et al., 2016b). LFQ intensity values were log2 transformed and potential contaminants and proteins identified by site only or reverse peptide were removed. Samples were grouped in experimental categories and proteins not identified in

4 out of 4 replicates in at least one group were also removed. Missing values were imputed using normally distributed values with a 1.8 downshift (log2) and a randomized 0.3 width (log2) considering whole matrix values. For the SUMO binders, the heatmap was based on Z-scores, and Volcano plots and Student's t tests with a permutation based FDR = 0.05 and an S0 = 0.1 were performed. For the GFP-XRCC4 interactome, volcano plots comparing wild-type and SIM mutants were constructed considering only significant GFP-XRCC4 interactors compared to GFP-only negative control. Student's t tests were performed with an FDR = 0.05 and an S0 = 0.1.

Statistical analysis tables were exported and processed in MS Excel, for further filtering and processing of the data.

For data visualization and STRING analysis, significant hits were analyzed in Cytoscape v3.7.0, using stringApp v1.4.0 and MCODE v1.5.1. Gene Ontology analysis was performed using the PANTHER overrepresentation test from the Gene Ontology Consortium.

4

Quantification of immunoblotting and microscopy data was performed using Fiji – ImageJ distribution and LAS-X, respectively. Statistical analysis of data was performed using GraphPad Prism 8 and Microsoft Excel software. Statistical details of individual experiments can be found in the figure legends, including the statistical test performed and definition of center and dispersion represented. For every analysis, N represents the number of values considered in the statistical analysis.

MATERIALS AVAILABILITY

All unique/stable reagents generated in this study are available from the Lead Contact upon reasonable request.

DATA AND CODE AVAILABILITY

The mass spectrometry proteomics data have been deposited to the ProteomeXchange Consortium via the PRIDE partner repository (Perez-Riverol et al., 2019) with the dataset identifiers PXD013842 (SUMO binders), PXD013844 (SUMO1 sites) and PXD022924 (GFP-XRCC4 interactors).

ACKNOWLEDGEMENTS

AUTHOR CONTRIBUTIONS

A.C.O.V., K.E.-O., and R.G.-P. conceived the project and designed the experiments. R.G.-P., K.E.-O., L.A.C., and E.W. conducted experiments in the laboratory of A.C.O.V. K.E.-O. conducted experiments in the laboratory of H.D.U. Z.X. prepared the SUMO1 sites samples. R.G.-P. acquired and analyzed the MS-based proteomics data. SIM peptides were synthesized by C.M.P.T.O. in the laboratory of H.O. R.G.-P. and A.C.O.V. wrote the manuscript, with input from K.E.-O. and H.D.U.

DECLARATION OF INTERESTS

H.O. is a co-founder of and shareholder in UbiQ Bio B.V., a company that markets research reagents. All of the other authors declare no competing interests.

REFERENCES

- Aguilar-Martinez, E., Chen, X., Webber, A., Mould, A.P., Seifert, A., Hay, R.T., and Sharrocks, A.D. (2015). Screen for multi-SUMO-binding proteins reveals a multi-SIM-binding mechanism for recruitment of the transcriptional regulator ZMYM2 to chromatin. Proc. Natl. Acad. Sci. U S A 112, E4854-4863.
- Anamika, and Spyracopoulos, L. (2016). Molecular Basis for Phosphorylation-dependent SUMO Recognition by the DNA Repair Protein RAP80. J. Biol. Chem. 291, 4417-4428.
- Arriagada, G., Muntean, L.N., and Goff, S.P. (2011). SUMO-interacting motifs of human TRIM5alpha are important for antiviral activity. PLoS Pathog. 7, e1002019.
- Banani, S.F., Rice, A.M., Peeples, W.B., Lin, Y., Jain, S., Parker, R., and Rosen, M.K. (2016). Compositional Control of Phase-Separated Cellular Bodies. Cell 166, 651-663.
- Cappadocia, L., and Lima, C.D. (2018). Ubiquitin-like Protein Conjugation: Structures, Chemistry, and Mechanism. Chem. Rev. 118, 889-918.
- Cappadocia, L., Pichler, A., and Lima, C.D. (2015). Structural basis for catalytic activation by the human ZNF451 SUMO E3 ligase. Nat. Struct. Mol. Biol. 22, 968-975.
- Chang, H.H.Y., Pannunzio, N.R., Adachi, N., and Lieber, M.R. (2017). Non-homologous DNA end joining and alternative pathways to double-strand break repair. Nat. Rev. Mol. Cell Biol. 18, 495-506.
- Cho, G., Lim, Y., and Golden, J.A. (2009). SUMO interaction motifs in Sizn1 are required for promyelocytic leukemia protein nuclear body localization and for transcriptional activation. J. Biol. Chem. 284, 19592-19600.
- Cho, S., Park, J.S., and Kang, Y.K. (2013). Regulated nuclear entry of over-expressed Setdb1. Genes Cells 18, 694-703.
- Colaert, N., Helsens, K., Martens, L., Vandekerckhove, J., and Gevaert, K. (2009). Improved visualization of protein consensus sequences by iceLogo. Nat. Methods 6, 786-787.
- Cong, L., Pakala, S.B., Ohshiro, K., Li, D.Q., and Kumar, R. (2011). SUMOylation and SUMO-interacting motif (SIM) of metastasis tumor antigen 1 (MTA1) synergistically regulate its transcriptional repressor function. J. Biol. Chem. 286, 43793-43808.
- Cox, E., Hwang, W., Uzoma, I., Hu, J., Guzzo, C.M., Jeong, J., Matunis, M.J., Qian, J., Zhu, H., and Blackshaw, S. (2017). Global Analysis of SUMO-Binding Proteins Identifies SUMOylation as a Key Regulator of the INO80 Chromatin Remodeling Complex. Mol. Cell. Proteomics 16, 812-823.
- Da Silva-Ferrada, E., Xolalpa, W., Lang, V., Aillet, F., Martin-Ruiz, I., de la Cruz-Herrera, C.F., Lopitz-Otsoa, F., Carracedo, A., Goldenberg, S.J., Rivas, C., et al. (2013). Analysis of SUMOylated proteins using SUMO-traps. Sci. Rep. 3, 1690.
- Danielsen, J.R., Povlsen, L.K., Villumsen, B.H., Streicher, W., Nilsson, J., Wikstrom, M., Bekker-Jensen, S., and Mailand, N. (2012). DNA damage-inducible SUMOylation of HERC2 promotes RNF8 binding via a novel SUMO-binding Zinc finger. J. Cell Biol. 197, 179-187.
- de la Cruz-Herrera, C.F., Baz-Martinez, M., Motiam, A.E., Vidal, S., Collado, M., Vidal, A., Rodriguez, M.S., Esteban, M., and Rivas, C. (2017). Phosphorylable tyrosine residue 162 in the double-stranded RNA-dependent kinase PKR modulates its interaction with SUMO. Sci. Rep. 7, 14055.
- Deribe, Y.L., Pawson, T., and Dikic, I. (2010). Post-translational modifications in signal integration. Nat. Struct. Mol. Biol. 17, 666-672.
- Diehl, C., Akke, M., Bekker-Jensen, S., Mailand, N., Streicher, W., and Wikstrom, M. (2016). Structural Analysis of a Complex between Small Ubiquitin-like Modifier 1 (SUMO1) and the ZZ Domain of CREB-binding Protein (CBP/p300) Reveals a New Interaction Surface on SUMO. J. Biol. Chem. 291, 12658-12672.
- Du, J.X., McConnell, B.B., and Yang, V.W. (2010). A small ubiquitin-related modifier-interacting motif functions as the transcriptional activation domain of Kruppel-like factor 4. J. Biol. Chem. 285, 28298-28308.
- Eifler, K., Cuijpers, S.A.G., Willemstein, E., Raaijmakers, J.A., El Atmioui, D., Ovaa, H., Medema, R.H., and Vertegaal, A.C.O. (2018). SUMO targets the APC/C to regulate transition from metaphase to anaphase. Nat. Commun. 9, 1119.

4

- Eisenhardt, N., Chaugule, V.K., Koidl, S., Droescher, M., Dogan, E., Rettich, J., Sutinen, P., Imanishi, S.Y., Hofmann, K., Palvimo, J.J., et al. (2015). A new vertebrate SUMO enzyme family reveals insights into SUMO-chain assembly. Nat. Struct. Mol. Biol. 22, 959-967.
- Escobar-Cabrera, E., Okon, M., Lau, D.K., Dart, C.F., Bonvin, A.M., and McIntosh, L.P. (2011). Characterizing the N- and C-terminal Small ubiquitin-like modifier (SUMO)-interacting motifs of the scaffold protein DAXX. J. Biol. Chem. 286, 19816-19829.
- Flotho, A., and Melchior, F. (2013). Sumoylation: a regulatory protein modification in health and disease. Annu. Rev. Biochem. 82, 357-385.
- Galanty, Y., Belotserkovskaya, R., Coates, J., and Jackson, S.P. (2012). RNF4, a SUMO-targeted ubiquitin E3 ligase, promotes DNA double-strand break repair. Genes Dev. 26, 1179-1195.
- Galanty, Y., Belotserkovskaya, R., Coates, J., Polo, S., Miller, K.M., and Jackson, S.P. (2009). Mammalian SUMO E3-ligases PIAS1 and PIAS4 promote responses to DNA double-strand breaks. Nature 462, 935-939.
- Garzon, J., Rodriguez-Munoz, M., Vicente-Sanchez, A., Garcia-Lopez, M.A., Martinez-Murillo, R., Fischer, T., and Sanchez-Blazquez, P. (2011). SUMO-SIM interactions regulate the activity of RGSZ2 proteins. PLoS One 6, e28557.
- Golebiowski, F., Matic, I., Tatham, M.H., Cole, C., Yin, Y., Nakamura, A., Cox, J., Barton, G.J., Mann, M., and Hay, R.T. (2009). System-wide changes to SUMO modifications in response to heat shock. Sci. Signal. 2, ra24.
- Gonzalez-Prieto, R., Cuijpers, S.A., Luijsterburg, M.S., van Attikum, H., and Vertegaal, A.C. (2015). SUMOylation and PARylation cooperate to recruit and stabilize SLX4 at DNA damage sites. EMBO Rep. 16, 512-519.
- Guervilly, J.H., Takedachi, A., Naim, V., Scaglione, S., Chawhan, C., Lovera, Y., Despras, E., Kuraoka, I., Kannouche, P., Rosselli, F., et al. (2015). The SLX4 complex is a SUMO E3 ligase that impacts on replication stress outcome and genome stability. Mol. Cell 57, 123-137.
- Guo, C., Nakazawa, Y., Woodbine, L., Bjorkman, A., Shimada, M., Fawcett, H., Jia, N., Ohyama, K., Li, T.S., Nagayama, Y., et al. (2015). XRCC4 deficiency in human subjects causes a marked neurological phenotype but no overt immunodeficiency. J. Allergy Clin. Immunol. 136, 1007-1017.
- Guzzo, C.M., Ringel, A., Cox, E., Uzoma, I., Zhu, H., Blackshaw, S., Wolberger, C., and Matunis, M.J. (2014). Characterization of the SUMO-binding activity of the myeloproliferative and mental retardation (MYM)-type zinc fingers in ZNF261 and ZNF198. PLoS One 9, e105271.
- He, X., Riceberg, J., Soucy, T., Koenig, E., Minissale, J., Gallery, M., Bernard, H., Yang, X., Liao, H., Rabino, C., et al. (2017). Probing the roles of SUMOylation in cancer cell biology by using a selective SAE inhibitor. Nat. Chem. Biol. 13, 1164-1171.
- Hecker, C.M., Rabiller, M., Haglund, K., Bayer, P., and Dikic, I. (2006). Specification of SUMO1- and SUMO2-interacting motifs. J. Biol. Chem. 281, 16117-16127.
- Hendriks, I.A., D'Souza, R.C., Yang, B., Verlaan-de Vries, M., Mann, M., and Vertegaal, A.C. (2014). Uncovering global SUMOylation signaling networks in a site-specific manner. Nat. Struct. Mol. Biol. 21, 927-936.
- Hendriks, I.A., Lyon, D., Su, D., Skotte, N.H., Daniel, J.A., Jensen, L.J., and Nielsen, M.L. (2018). Site-specific characterization of endogenous SUMOylation across species and organs. Nat. Commun. 9, 2456.
- Hendriks, I.A., Lyon, D., Young, C., Jensen, L.J., Vertegaal, A.C., and Nielsen, M.L. (2017). Site-specific mapping of the human SUMO proteome reveals co-modification with phosphorylation. Nat. Struct. Mol. Biol. 24, 325-336.
- Hendriks, I.A., and Vertegaal, A.C. (2016). A comprehensive compilation of SUMO proteomics. Nat. Rev. Mol. Cell Biol. 17, 581-595.
- Hickey, C.M., Wilson, N.R., and Hochstrasser, M. (2012). Function and regulation of SUMO proteases. Nat. Rev. Mol. Cell Biol. 13, 755-766.
- Hietakangas, V., Anckar, J., Blomster, H.A., Fujimoto, M., Palvimo, J.J., Nakai, A., and Sistonen, L. (2006). PDSM, a motif for phosphorylation-dependent SUMO modification. Proc. Natl. Acad. Sci. U S A 103, 45-50.

- Hong, T.T., Smyth, J.W., Gao, D., Chu, K.Y., Vogan, J.M., Fong, T.S., Jensen, B.C., Colecraft, H.M., and Shaw, R.M. (2010). BIN1 localizes the L-type calcium channel to cardiac T-tubules. PLoS Biol. 8, e1000312.
- Husnjak, K., and Dikic, I. (2012). Ubiquitin-binding proteins: decoders of ubiquitin-mediated cellular functions. Annu. Rev. Biochem. 81, 291-322.
- Hwang, S.P., and Lee, D.H. (2017). Autophagy mediates SUMO-induced degradation of a polyglutamine protein ataxin-3. Anim. Cells. Syst. (Seoul) 21, 169-176.
- Impens, F., Radoshevich, L., Cossart, P., and Ribet, D. (2014). Mapping of SUMO sites and analysis of SUMOylation changes induced by external stimuli. Proc. Natl. Acad. Sci. U S A 111, 12432-12437.
- Jentsch, S., and Psakhye, I. (2013). Control of nuclear activities by substrate-selective and protein-group SUMOylation. Annu. Rev. Genet. 47, 167-186.
- Johnson, E.S., and Blobel, G. (1999). Cell cycle-regulated attachment of the ubiquitin-related protein SUMO to the yeast septins. J. Cell Biol. 147, 981-994.
- Kaur, K., Park, H., Pandey, N., Azuma, Y., and De Guzman, R.N. (2017). Identification of a new small ubiquitin-like modifier (SUMO)-interacting motif in the E3 ligase PIASy. J. Biol. Chem. 292, 10230-10238.
- Kumar, R., Gonzalez-Prieto, R., Xiao, Z., Verlaan-de Vries, M., and Vertegaal, A.C.O. (2017). The STUbL RNF4 regulates protein group SUMOylation by targeting the SUMO conjugation machinery. Nat. Commun. 8, 1809.
- Lallemand-Breitenbach, V., Jeanne, M., Benhenda, S., Nasr, R., Lei, M., Peres, L., Zhou, J., Zhu, J., Raught, B., and de The, H. (2008). Arsenic degrades PML or PML-RARalpha through a SUMO-triggered RNF4/ubiquitin-mediated pathway. Nat. Cell Biol. 10, 547-555.
- Lecona, E., Rodriguez-Acebes, S., Specks, J., Lopez-Contreras, A.J., Ruppen, I., Murga, M., Munoz, J., Mendez, J., and Fernandez-Capetillo, O. (2016). USP7 is a SUMO deubiquitinase essential for DNA replication. Nat. Struct. Mol. Biol. 23, 270-277.
- Lee, K.J., Jovanovic, M., Udayakumar, D., Bladen, C.L., and Dynan, W.S. (2004). Identification of DNA-PKcs phosphorylation sites in XRCC4 and effects of mutations at these sites on DNA end joining in a cell-free system. DNA Repair (Amst) 3, 267-276.
- Lescasse, R., Pobiega, S., Callebaut, I., and Marcand, S. (2013). End-joining inhibition at telomeres requires the translocase and polySUMO-dependent ubiquitin ligase Uls1. EMBO J. 32, 805-815.
- Li, C., Peng, Q., Wan, X., Sun, H., and Tang, J. (2017). C-terminal motifs in promyelocytic leukemia protein isoforms critically regulate PML nuclear body formation. J. Cell Sci. 130, 3496-3506.
- Liebelt, F., Sebastian, R.M., Moore, C.L., Mulder, M.P.C., Ovaa, H., Shoulders, M.D., and Vertegaal, A.C.O. (2019). SUMOylation and the HSF1-Regulated Chaperone Network Converge to Promote Proteostasis in Response to Heat Shock. Cell Rep. 26, 236-249 e234.
- Mahajan, R., Delphin, C., Guan, T., Gerace, L., and Melchior, F. (1997). A small ubiquitin-related polypeptide involved in targeting RanGAP1 to nuclear pore complex protein RanBP2. Cell 88, 97-107.
- Mahajan, R., Gerace, L., and Melchior, F. (1998). Molecular characterization of the SUMO-1 modification of RanGAP1 and its role in nuclear envelope association. J. Cell. Biol. 140, 259-270.
- Martin, J.S., Winkelmann, N., Petalcorin, M.I., McIlwraith, M.J., and Boulton, S.J. (2005). RAD-51-dependent and -independent roles of a Caenorhabditis elegans BRCA2-related protein during DNA double-strand break repair. Mol. Cell. Biol. 25, 3127-3139.
- Matic, I., Schimmel, J., Hendriks, I.A., van Santen, M.A., van de Rijke, F., van Dam, H., Gnad, F., Mann, M., and Vertegaal, A.C. (2010). Site-specific identification of SUMO-2 targets in cells reveals an inverted SUMOylation motif and a hydrophobic cluster SUMOylation motif. Mol. Cell 39, 641-652.
- Matunis, M.J., Coutavas, E., and Blobel, G. (1996). A novel ubiquitin-like modification modulates the partitioning of the Ran-GTPase-activating protein RanGAP1 between the cytosol and the nuclear pore complex. J. Cell Biol. 135, 1457-1470.
- Matunis, M.J., Wu, J., and Blobel, G. (1998). SUMO-1 modification and its role in targeting the Ran GTPase-activating protein, RanGAP1, to the nuclear pore complex. J. Cell Biol. 140, 499-509.

4

- McLaughlin, D., Coey, C.T., Yang, W.C., Drohat, A.C., and Matunis, M.J. (2016). Characterizing Requirements for Small Ubiquitin-like Modifier (SUMO) Modification and Binding on Base Excision Repair Activity of Thymine-DNA Glycosylase in Vivo. J. Biol. Chem. 291, 9014-9024.
- Meng, F., Qian, J., Yue, H., Li, X., and Xue, K. (2016). SUMOylation of Rb enhances its binding with CDK2 and phosphorylation at early G1 phase. Cell Cycle 15, 1724-1732.
- Merrill, J.C., Melhuish, T.A., Kagey, M.H., Yang, S.H., Sharrocks, A.D., and Wotton, D. (2010). A role for non-covalent SUMO interaction motifs in Pc2/CBX4 E3 activity. PLoS One 5, e8794.
- Meulmeester, E., Kunze, M., Hsiao, H.H., Urlaub, H., and Melchior, F. (2008). Mechanism and consequences for paralog-specific sumoylation of ubiquitin-specific protease 25. Mol. Cell 30, 610-619.
- Moore, H.M., Bai, B., Boisvert, F.M., Latonen, L., Rantanen, V., Simpson, J.C., Pepperkok, R., Lamond, A.I., and Laiho, M. (2011). Quantitative proteomics and dynamic imaging of the nucleolus reveal distinct responses to UV and ionizing radiation. Mol. Cell. Proteomics 10, M111 009241.
- Morris, J.R., Boutell, C., Keppler, M., Densham, R., Weekes, D., Alamshah, A., Butler, L., Galanty, Y., Pangon, L., Kiuchi, T., et al. (2009). The SUMO modification pathway is involved in the BRCA1 response to genotoxic stress. Nature 462, 886-890.
- Murray, J.E., van der Burg, M., H, I.J., Carroll, P., Wu, Q., Ochi, T., Leitch, A., Miller, E.S., Kysela, B., Jawad, A., et al. (2015). Mutations in the NHEJ component XRCC4 cause primordial dwarfism. Am. J. Hum. Genet. 96, 412-424.
- Nacerddine, K., Lehembre, F., Bhaumik, M., Artus, J., Cohen-Tannoudji, M., Babinet, C., Pandolfi, P.P., and Dejean, A. (2005). The SUMO pathway is essential for nuclear integrity and chromosome segregation in mice. Dev. Cell 9, 769-779.
- Normanno, D., Negrel, A., de Melo, A.J., Betzi, S., Meek, K., and Modesti, M. (2017). Mutational phospho-mimicry reveals a regulatory role for the XRCC4 and XLF C-terminal tails in modulating DNA bridging during classical non-homologous end joining. Elife 6, e22900.
- Ochi, T., Wu, Q., and Blundell, T.L. (2014). The spatial organization of non-homologous end joining: from bridging to end joining. DNA Repair (Amst) 17, 98-109.
- Ouyang, J., Garner, E., Hallet, A., Nguyen, H.D., Rickman, K.A., Gill, G., Smogorzewska, A., and Zou, L. (2015). Noncovalent interactions with SUMO and ubiquitin orchestrate distinct functions of the SLX4 complex in genome maintenance. Mol. Cell 57, 108-122.
- Ouyang, J., Shi, Y., Valin, A., Xuan, Y., and Gill, G. (2009). Direct binding of CoREST1 to SUMO-2/3 contributes to gene-specific repression by the LSD1/CoREST1/HDAC complex. Mol. Cell 34, 145-154.
- Pawson, T. (2004). Specificity in signal transduction: from phosphotyrosine-SH2 domain interactions to complex cellular systems. Cell 116, 191-203.
- Perez-Riverol, Y., Csordas, A., Bai, J., Bernal-Llinares, M., Hewapathirana, S., Kundu, D.J., Inuganti, A., Griss, J., Mayer, G., Eisenacher, M., et al. (2019). The PRIDE database and related tools and resources in 2019: improving support for quantification data. Nucleic Acids Res. 47, D442-D450.
- Prudden, J., Pebernard, S., Raffa, G., Slavin, D.A., Perry, J.J., Tainer, J.A., McGowan, C.H., and Boddy, M.N. (2007). SUMO-targeted ubiquitin ligases in genome stability. EMBO J. 26, 4089-4101.
- Psakhye, I., and Jentsch, S. (2012). Protein group modification and synergy in the SUMO pathway as exemplified in DNA repair. Cell 151, 807-820.
- Rappsilber, J., Mann, M., and Ishihama, Y. (2007). Protocol for micro-purification, enrichment, pre-fractionation and storage of peptides for proteomics using StageTips. Nat. Protoc. 2, 1896-1906.
- Saether, T., Pattabiraman, D.R., Alm-Kristiansen, A.H., Vogt-Kielland, L.T., Gonda, T.J., and Gabrielsen, O.S. (2011). A functional SUMO-interacting motif in the transactivation domain of c-Myb regulates its myeloid transforming ability. Oncogene 30, 212-222.
- Sahin, U., Ferhi, O., Jeanne, M., Benhenda, S., Berthier, C., Jollivet, F., Niwa-Kawakita, M., Faklaris, O., Setterblad, N., de The, H., et al. (2014). Oxidative stress-induced assembly of PML nuclear bodies controls sumoylation of partner proteins. J. Cell Biol. 204, 931-945.

- Sahoo, M.R., Gaikwad, S., Khuperkar, D., Ashok, M., Helen, M., Yadav, S.K., Singh, A., Magre, I., Deshmukh, P., Dhanvijay, S., et al. (2017). Nup358 binds to AGO proteins through its SUMO-interacting motifs and promotes the association of target mRNA with miRISC. EMBO Rep. 18, 241-263.
- Saitoh, H., and Hinchey, J. (2000). Functional heterogeneity of small ubiquitin-related protein modifiers SUMO-1 versus SUMO-2/3. J. Biol. Chem. 275, 6252-6258.
- Santiago, A., Godsey, A.C., Hossain, J., Zhao, L.Y., and Liao, D. (2009). Identification of two independent SUMO-interacting motifs in Daxx: evolutionary conservation from Drosophila to humans and their biochemical functions. Cell Cycle 8, 76-87.
- Schellenberg, M.J., Lieberman, J.A., Herrero-Ruiz, A., Butler, L.R., Williams, J.G., Munoz-Cabello, A.M., Mueller, G.A., London, R.E., Cortes-Ledesma, F., and Williams, R.S. (2017). ZATT (ZNF451)-mediated resolution of topoisomerase 2 DNA-protein cross-links. Science 357, 1412-1416.
- Seenivasan, R., Hermanns, T., Blyszcz, T., Lammers, M., Praefcke, G.J.K., and Hofmann, K. (2019). Mechanism and chain specificity of RNF216/TRIAD3, the ubiquitin ligase mutated in Gordon Holmes syndrome. Hum. Mol. Genet. 28, 2862-2873.
- Sekiyama, N., Ikegami, T., Yamane, T., Ikeguchi, M., Uchimura, Y., Baba, D., Ariyoshi, M., Tochio, H., Saitoh, H., and Shirakawa, M. (2008). Structure of the small ubiquitin-like modifier (SUMO)-interacting motif of MBD1-containing chromatin-associated factor 1 bound to SUMO-3. J. Biol. Chem. 283, 35966-35975.
- Sharma, M.K., Imamichi, S., Fukuchi, M., Samarth, R.M., Tomita, M., and Matsumoto, Y. (2016). In cellulo phosphorylation of XRCC4 Ser320 by DNA-PK induced by DNA damage. J. Radiat. Res. 57, 115-120.
- Shen, T.H., Lin, H.K., Scaglioni, P.P., Yung, T.M., and Pandolfi, P.P. (2006). The mechanisms of PML-nuclear body formation. Mol. Cell 24, 331-339.
- Sibanda, B.L., Critchlow, S.E., Begun, J., Pei, X.Y., Jackson, S.P., Blundell, T.L., and Pellegrini, L. (2001). Crystal structure of an Xrcc4-DNA ligase IV complex. Nat. Struct. Biol. 8, 1015-1019.
- Sridharan, V., and Azuma, Y. (2016). SUMO-interacting motifs (SIMs) in Polo-like kinase 1-interacting checkpoint helicase (PICH) ensure proper chromosome segregation during mitosis. Cell Cycle 15, 2135-2144.
- Sriramachandran, A.M., Meyer-Teschendorf, K., Pabst, S., Ulrich, H.D., Gehring, N.H., Hofmann, K., Praefcke, G.J.K., and Dohmen, R.J. (2019). Arkadia/RNF111 is a SUMO-targeted ubiquitin ligase with preference for substrates marked with SUMO1-capped SUMO2/3 chain. Nat. Commun. 10, 3678.
- Sun, H., Liu, Y., and Hunter, T. (2014). Multiple Arkadia/RNF111 structures coordinate its Polycomb body association and transcriptional control. Mol. Cell. Biol. 34, 2981-2995.
- Sung, K.S., Lee, Y.A., Kim, E.T., Lee, S.R., Ahn, J.H., and Choi, C.Y. (2011). Role of the SUMO-interacting motif in HIPK2 targeting to the PML nuclear bodies and regulation of p53. Exp. Cell Res. 317, 1060-1070.
- Swatek, K.N., and Komander, D. (2016). Ubiquitin modifications. Cell Res. 26, 399-422.
- Szklarczyk, D., Franceschini, A., Wyder, S., Forslund, K., Heller, D., Huerta-Cepas, J., Simonovic, M., Roth, A., Santos, A., Tsafou, K.P., et al. (2015). STRING v10: protein-protein interaction networks, integrated over the tree of life. Nucleic Acids Res. 43, D447-452.
- Tammsalu, T., Matic, I., Jaffray, E.G., Ibrahim, A.F.M., Tatham, M.H., and Hay, R.T. (2014). Proteome-wide identification of SUMO2 modification sites. Sci. Signal. 7, rs2.
- Tapia, O., Lafarga, V., Bengoechea, R., Palanca, A., Lafarga, M., and Berciano, M.T. (2014). The SMN Tudor SIM-like domain is key to SmD1 and coilin interactions and to Cajal body biogenesis. J. Cell Sci. 127, 939-946.
- Tatham, M.H., Geoffroy, M.C., Shen, L., Plechanovova, A., Hattersley, N., Jaffray, E.G., Palvimo, J.J., and Hay, R.T. (2008). RNF4 is a poly-SUMO-specific E3 ubiquitin ligase required for arsenic-induced PML degradation. Nat. Cell Biol. 10, 538-546.
- Tyanova, S., Temu, T., and Cox, J. (2016a). The MaxQuant computational platform for mass spectrometry-based shotgun proteomics. Nat. Protoc. 11, 2301-2319.

4

- Tyanova, S., Temu, T., Sinitcyn, P., Carlson, A., Hein, M.Y., Geiger, T., Mann, M., and Cox, J. (2016b). The Perseus computational platform for comprehensive analysis of (prote)omics data. Nat. Methods 13, 731-740.
- Vertegaal, A.C., Andersen, J.S., Ogg, S.C., Hay, R.T., Mann, M., and Lamond, A.I. (2006). Distinct and overlapping sets of SUMO-1 and SUMO-2 target proteins revealed by quantitative proteomics. Mol. Cell. Proteomics 5, 2298-2310.
- Vyas, R., Kumar, R., Clermont, F., Helfricht, A., Kalev, P., Sotiropoulou, P., Hendriks, I.A., Radaelli, E., Hochepied, T., Blanpain, C., et al. (2013). RNF4 is required for DNA double-strand break repair in vivo. Cell Death Differ. 20, 490-502.
- Wang, C.H., Hung, P.W., Chiang, C.W., Lombes, M., Chen, C.H., Lee, K.H., Lo, Y.C., Wu, M.H., Chang, W.C., and Lin, D.Y. (2019). Identification of two independent SUMO-interacting motifs in Fas-associated factor 1 (FAF1): Implications for mineralocorticoid receptor (MR)-mediated transcriptional regulation. Biochim Biophys Acta Mol. Cell Res. 1866, 1282-1297.
- Yang, K., Guo, R., and Xu, D. (2016). Non-homologous end joining: advances and frontiers. Acta Biochim. Biophys. Sin. (Shanghai) 48, 632-640.
- Yang, S.H., Galanis, A., Witty, J., and Sharrocks, A.D. (2006). An extended consensus motif enhances the specificity of substrate modification by SUMO. EMBO J. 25, 5083-5093.
- Yang, X., Boehm, J.S., Yang, X., Salehi-Ashtiani, K., Hao, T., Shen, Y., Lubonja, R., Thomas, S.R., Alkan, O., Bhimdi, T., et al. (2011). A public genome-scale lentiviral expression library of human ORFs. Nat. Methods 8, 659-661.
- Yin, Y., Seifert, A., Chua, J.S., Maure, J.F., Golebiowski, F., and Hay, R.T. (2012). SUMO-targeted ubiquitin E3 ligase RNF4 is required for the response of human cells to DNA damage. Genes Dev. 26, 1196-1208.
- Yu, Y., Wang, W., Ding, Q., Ye, R., Chen, D., Merkle, D., Schriemer, D., Meek, K., and Lees-Miller, S.P. (2003). DNA-PK phosphorylation sites in XRCC4 are not required for survival after radiation or for V(D)J recombination. DNA Repair (Amst) 2, 1239-1252.
- Zhang, X.D., Goeres, J., Zhang, H., Yen, T.J., Porter, A.C., and Matunis, M.J. (2008). SUMO-2/3 modification and binding regulate the association of CENP-E with kinetochores and progression through mitosis. Mol. Cell 29, 729-741.
- Zhang, Z., Du, J., Wang, S., Shao, L., Jin, K., Li, F., Wei, B., Ding, W., Fu, P., van Dam, H., et al. (2019). OTUB2 Promotes Cancer Metastasis via Hippo-Independent Activation of YAP and TAZ. Mol. Cell 73, 7-21 e27.
- Zhao, Q., Xie, Y., Zheng, Y., Jiang, S., Liu, W., Mu, W., Liu, Z., Zhao, Y., Xue, Y., and Ren, J. (2014). GPS-SUMO: a tool for the prediction of sumoylation sites and SUMO-interaction motifs. Nucleic Acids Res. 42, W325-330.
- Zheng, N., and Shabek, N. (2017). Ubiquitin Ligases: Structure, Function, and Regulation. Annu. Rev. Biochem. 86, 129-157.
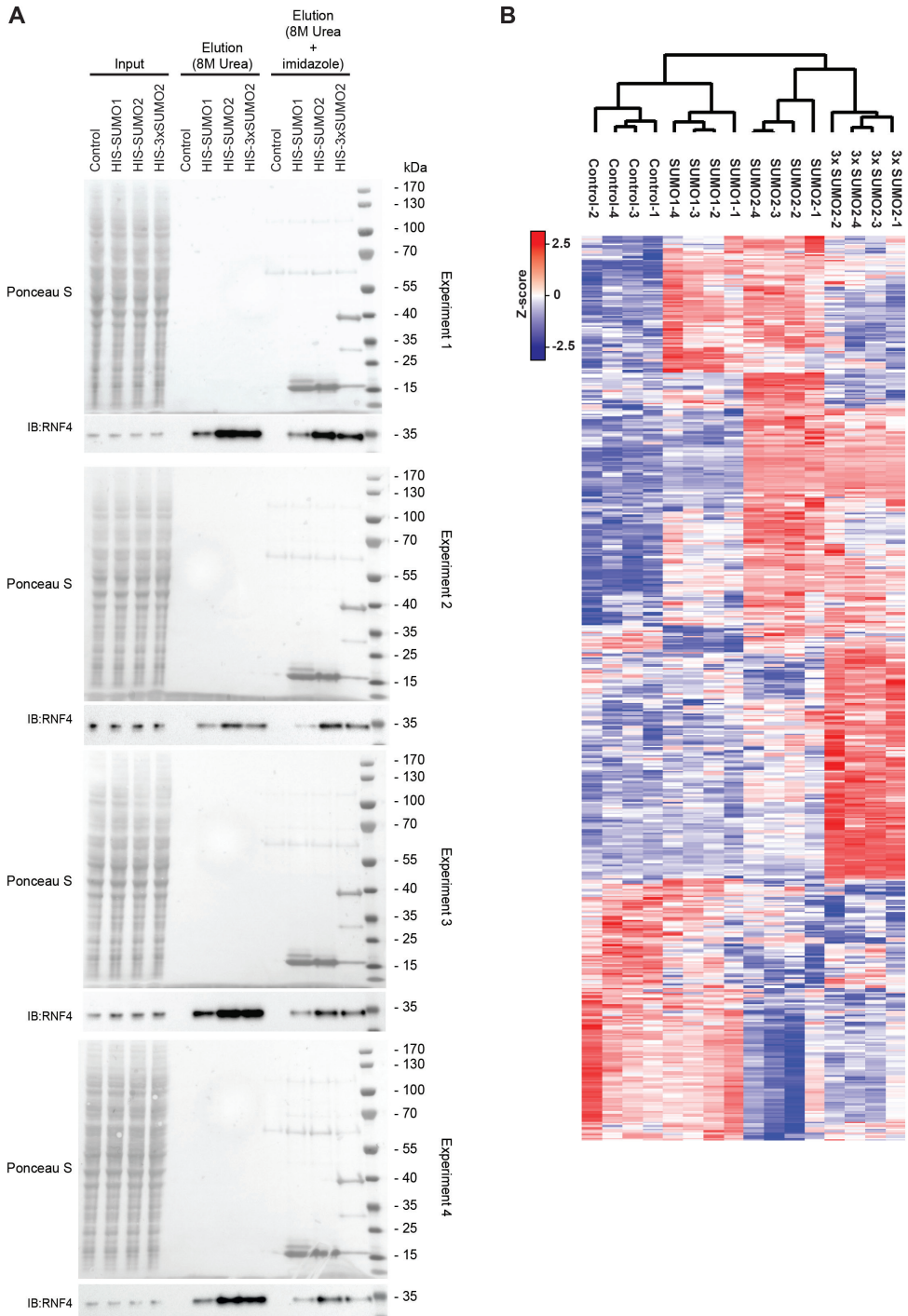
Figure S1. Purification and identification of SUMO isoform-specific binders. Related to Figure 1.

Figure S1 *(continued).*
(A) Immunoblotting analysis of the four replicates of the SUMO-binding screen. RNF4 was used as a positive control for SUMO binding proteins. **(B)** Heatmap analysis of the four replicates including proteins identified in four replicates in at least one condition and excluding background binders (not significant for ANOVA FDR=0.05 S0=0.1), confirming reproducibility of the data. Enriched proteins are indicated in red.

Figure S2. Analysis of SUMO2-binders. Related to Figure 2. STRING network analysis of SUMO2 binders including connected and unconnected nodes. The size of the circle represents the-Log p-value of the identification as binder. Red color intensity represents the average enrichment compared to control beads. Dotted lines indicate that the protein is a SUMO2-specific binder.
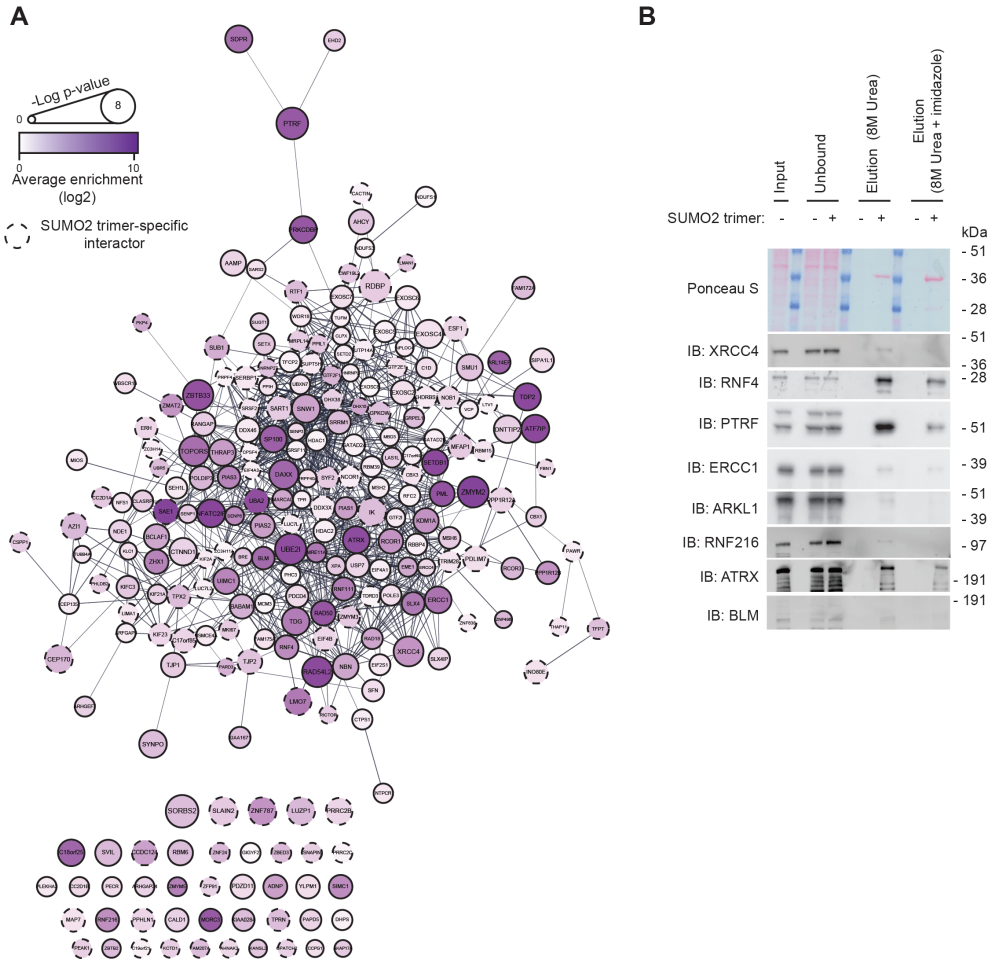
Figure S3. Analysis of SUMO2 trimer binders. Related to Figure 3. (A) STRING network analysis of SUMO2 trimer binders including connected and unconnected nodes. The size of the circle represents the-Log p-value of the identification as binder. Violet color intensity represents the average enrichment compared to control beads. Dotted lines indicate that the protein is a SUMO2 trimer specific binder. **(B)** Confirmation by immunoblotting of SUMO2 trimer-binding proteins identified by mass spectrometry. NiNTA beads were coated or not with SUMO2 trimer and incubated with a Hela lysate. Binding proteins were eluted by denaturing with 8 M Urea and subsequently 8 M Urea containing 500 mM Imidazole, to also release SUMO2 trimers from the beads. The experiment was performed twice.
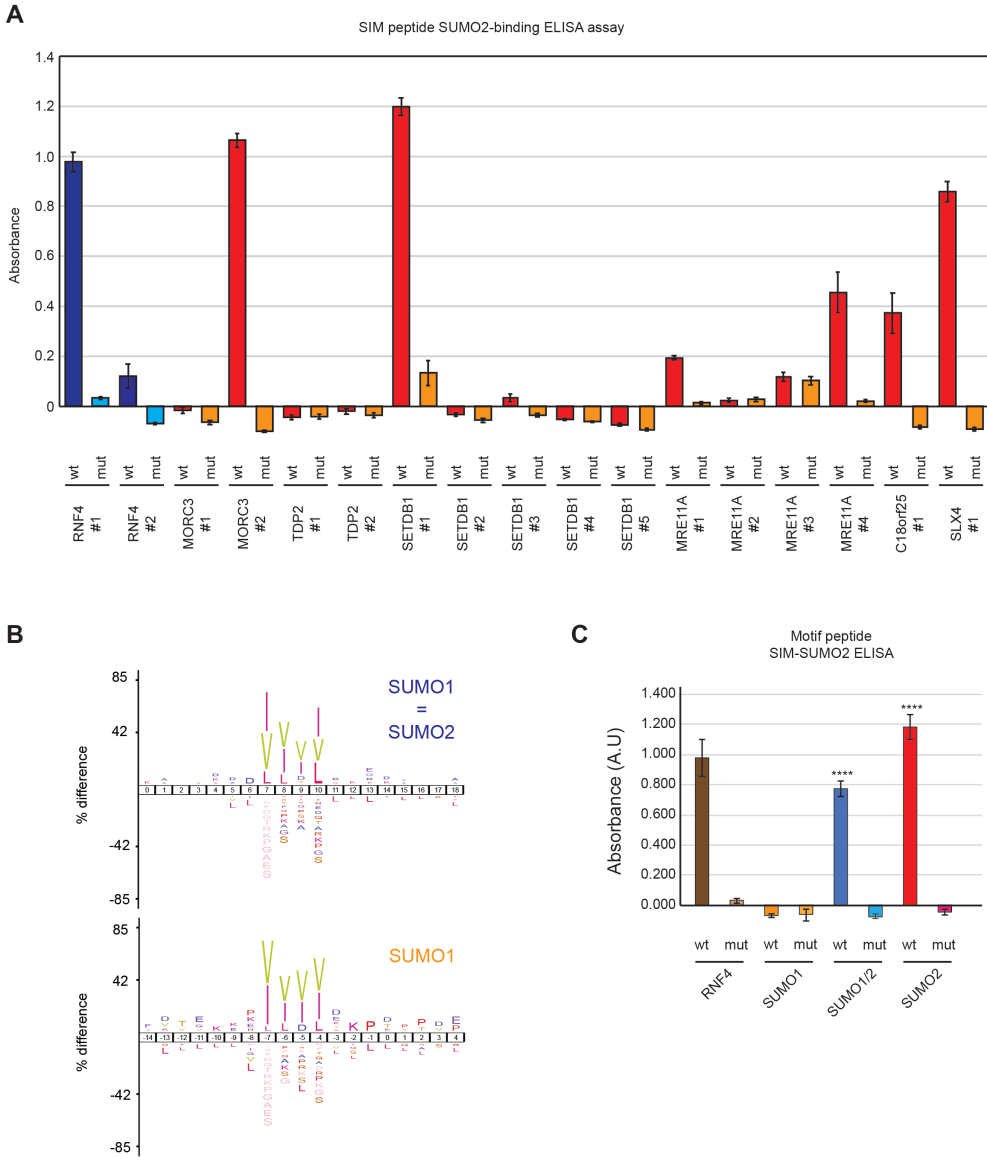
Figure S4. Towards a more efficient SUMO2 trap. Related to Figure 5. (A) Results from the SUMO2-trimer binding ELISA of selected SIM-containing peptides and their controls as indicated in Table 1. Average and standard deviation of three independent experiments in triplicate (n=9) are shown. **(B)** IceLogos of predicted SIMs from either preferential SUMO1 binders or binders with no preference for SUMO1 or SUMO2. **(C)** Results from the SUMO2-trimer ELISA using SIM-containing peptides and their controls with a predicted preference for SUMO1, SUMO2, or no preference from Table 1. Average and standard deviation of three independent experiments in triplicate (n=9) are shown.
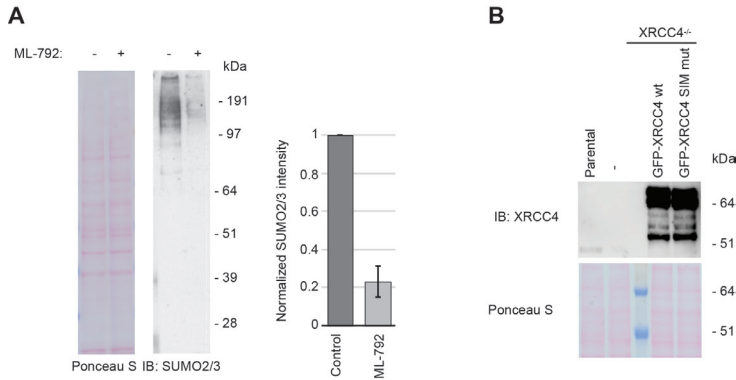
Figure S5. A SIM in XRCC4 is important for its recruitment to DNA damage sites. Related to Figure 6. **(A)** SUMO2/3 levels determined by immunoblot analysis of U2OS cells expressing GFP-XRCC4 and KU70-mCherry, which were treated for 4h with 1 μM SUMO E1 inhibitor ML-792 or left untreated. Ponceau S is provided as loading control. Normalized average SUMO2 intensity and standard deviation from three independent experiments are shown. **(B)** Immunoblot of parental and XRCC4-/- cells rescued with GFP-XRCC4$_{wt}$ and GFP-XRCC4$_{SIM}$ mutant.
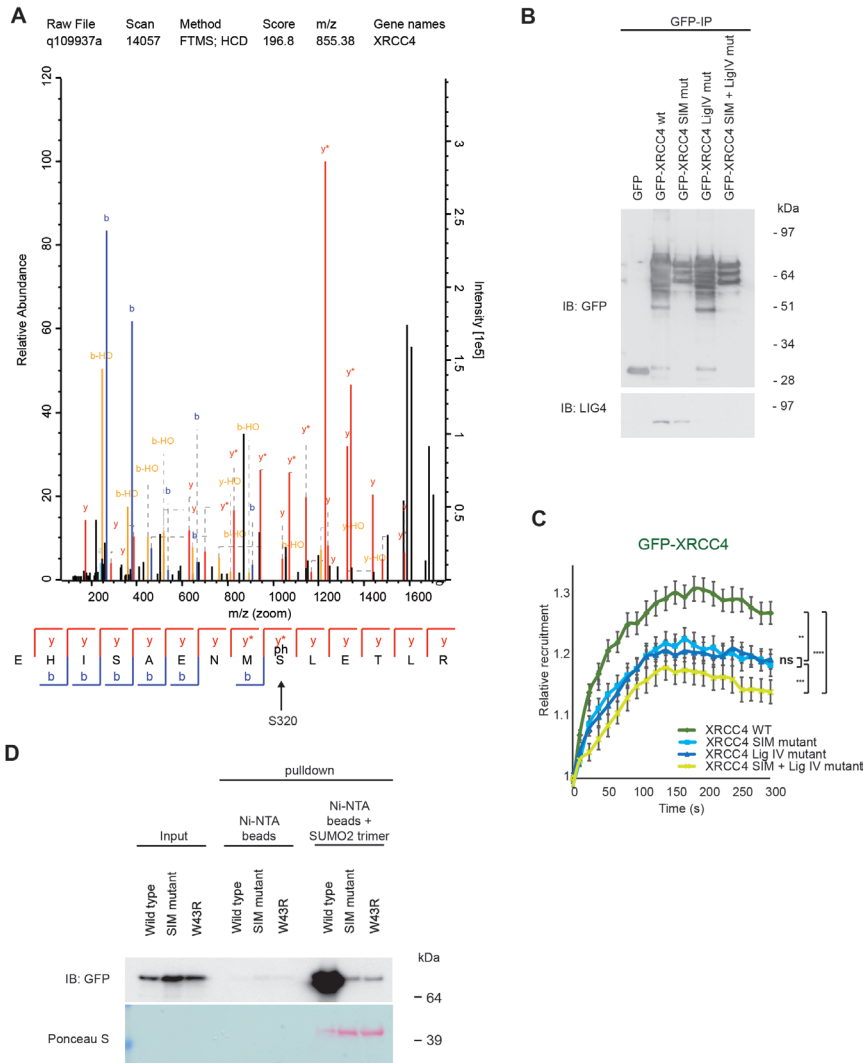
Figure S6. A SIM in XRCC4 is important for its recruitment to DNA damage sites. Related to Figures 6 and 7. (A) Best MS/MS spectrum of XRCC4 tryptic peptide containing phosphorylated Serine 320. **(B)** U2OS cells were transiently transfected with either wild type, SIM mutant, Ligase IV mutant or SIM+Ligase IV double mutant GFP-XRCC4 constructs. GFP-XRCC4 interaction with Ligase IV for the different constructs was analyzed by immunoblotting. **(C)** Quantification of the relative recruitment of different GFP-XRCC4 constructs to DNA damage sites induced by laser micro-irradiation. Curves represent mean relative recruitment and error bars represent the SEM of values from two or more independent experiments (N_{wt}=74; N_{SIM}=73; N_{LigIV}=93, $N_{SIM+LigIV}$=65). Kruskal-Wallis tests were performed to determine statistical differences using the Area Under the Curve (AUC) (*p<0.05; **p<0.01; ***p<0.001; ****p<0.0001). **(D)** Affinity of different GFP-XRCC4 wild-type, SIM-mutant and W43R constructs for SUMO2 trimers. Lysates from U2OS cells expressing either GFP-XRCC4 wild-type, SIM-mutant, or W43R mutant constructs were incubated with Ni-NTA beads coated or not with HIS-SUMO2 trimer, washed and eluted. The amount of GFP-XRCC4 bound to the beads was investigated by immunoblotting. The experiment was performed three times.
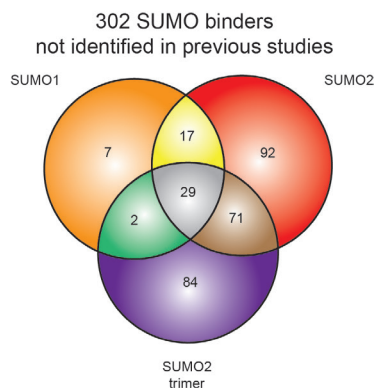
Figure S7. SUMO binders not identified in previous studies. Related to Figures 1-3. Venn diagram of 303 SUMO-binding proteins not previously identified in SUMO interactome papers (Aguilar-Martinez et al., 2015; Cox et al., 2017; Hecker et al., 2006; Ouyang et al., 2009) nor in individual studies (Aguilar-Martinez et al., 2015; Anamika and Spyracopoulos, 2016; Arriagada et al., 2011; Cappadocia et al., 2015; Cho et al., 2009; Cho et al., 2013; Cong et al., 2011; Danielsen et al., 2012; de la Cruz-Herrera et al., 2017; Diehl et al., 2016; Du et al., 2010; Eisenhardt et al., 2015; Escobar-Cabrera et al., 2011; Garzon et al., 2011; Guervilly et al., 2015; Guzzo et al., 2014; Hickey et al., 2012; Hwang and Lee, 2017; Kaur et al., 2017; Lecona et al., 2016; Li et al., 2017; McLaughlin et al., 2016; Meng et al., 2016; Merrill et al., 2010; Meulmeester et al., 2008; Ouyang et al., 2009; Saether et al., 2011; Sahoo et al., 2017; Santiago et al., 2009; Schellenberg et al., 2017; Seenivasan et al., 2019; Sekiyama et al., 2008; Sridharan and Azuma, 2016; Sriramachandran et al., 2019; Sun et al., 2014; Sung et al., 2011; Tapia et al., 2014; Tatham et al., 2008; Wang et al., 2019; Zhang et al., 2008; Zhang et al., 2019).

4